

## Precisely designed cobalt single atom on ZrO<sub>2</sub> support for chemical CO<sub>2</sub> fixation

Neha Choudhary<sup>a</sup>, Shan Jiang<sup>b</sup>, Hien Pham<sup>c</sup>, Gotluru Kedarnath<sup>d</sup>, Abhaya Datye\*<sup>c</sup>, Jeffrey T. Miller\*<sup>b</sup>, Avesh Kumar Tyagi\*<sup>d</sup>, Shaikh M. Mobin\*<sup>a,e</sup>

<sup>a</sup>Department of Chemistry, Indian Institute of Technology-Indore, Simrol, Khandwa Road, 433552, India.

<sup>b</sup>Davidson School of Chemical Engineering, Purdue University, West Lafayette, Indiana 47907, United States.

<sup>c</sup>Department of Chemical Biological Engineering and Center for Micro-Engineered Materials, University of New Mexico, Albuquerque, New Mexico 87131, United States

<sup>d</sup>Chemistry Division, Bhabha Atomic Research Centre, Mumbai 400085, India and Homi Bhabha National Institute, Anushaktinagar, Mumbai 400094, India

<sup>e</sup>Center for Advanced Electronics, Indian Institute of Technology-Indore, Simrol, Khandwa road, 433552, India.

\*Email: [xray@iiti.ac.in](mailto:xray@iiti.ac.in)

## Abstract

The presence of single atoms as active sites on a metal oxide support can dramatically enhance catalytic activity. Here, we demonstrate that Cobalt doped  $\text{ZrO}_2$  constitutes a single atom catalyst where each  $\text{Co}^{+2}$  ion act as active for  $\text{CO}_2$  fixation. The synthesized  $\text{Co}/\text{ZrO}_2$  catalyst was characterized by EXAFS and STEM to confirm the presence of isolated  $\text{Co}^{+2}$  on the  $\text{ZrO}_2$  support. The STEM-EDS data showed a uniform distribution of Co over the surface of the  $\text{ZrO}_2$  support. The catalytic results reveal that Co active sites on  $\text{ZrO}_2$  enhance catalytic performance and provide  $\sim 100\%$  conversion into carbonate products in the presence of trace amounts of tetrabutylammonium bromide (TBAB). When undoped  $\text{ZrO}_2$  and  $\text{Co}_3\text{O}_4$  impregnated  $\text{ZrO}_2$  catalyst was utilized for comparison, less than 50% conversion of epoxides was obtained. The single atom catalyst (SAC) showed a broad substrate scope, solvent-free reaction and higher catalytic activity and selectivity.

**Keywords:** Single atom catalyst;  $\text{CO}_2$  fixation; Solvent-free; recyclable catalyst; Co doped  $\text{ZrO}_2$  catalyst

## 1. Introduction

Heterogeneous catalysis has entered a new phase with the development of single-atom catalysts (SACs), in which the isolated active metal atoms are anchored to supports.[1–4] In SACs, every surface atomic site is accessible which delivers superior catalytic performance and the highest atom utilization efficiency.[5,6] SACs act as a bridge between homogeneous and heterogeneous catalysts as they possess properties of both type of materials i.e. recyclability and easy recoverability, thermal stability and better exposure of active sites. For industrial applications, recyclability, cost-effectiveness and catalytic performance are the key requirements. In comparison to nanoparticle catalysts, SACs have demonstrated impressive enhancements in catalytic activity in various catalytic processes due to their distinct structural characteristics and fully exposed active sites.[7–10] However, the synthesis and stabilization of SACs is a challenging task due to the high surface energy of the isolated atoms, resulting in aggregation of SACs and decrease in catalytic activity.[11–13] For synthesizing SACs, various strategies like doping, utilization of defects and spatial confinement have been utilized to stabilize the single atom over different supports.[11,14,15] Moreover, characterization of SACs remains a daunting task since it requires atomic level high resolution in techniques like STEM-HAADF and EELS. The conventional transmission electron microscopes are unable to observe single atoms on supported materials owing to their contrast mechanisms.[16] Aberration-corrected HAADF-STEM is extremely sensitive to atomic number of the atoms present in the sample. However, it is still challenging to observe single atoms when the difference in atomic numbers of the isolated atoms and the support is not enough to provide sufficient contrast.[17] Since AC-STEM is a local technique, it is necessary to combine information with techniques that provide an average over the entire sample, like EXAFS, and XANES while also yielding information on oxidation states and bond distances for nearest neighbors for the supported single atoms.[18]

Recently, SACs were explored for electrocatalytic, thermal and photocatalytic  $\text{CO}_2$  hydrogenation and valorization reactions due to their enhanced catalytic performance.[4,19–23] SACs provide more exposure to active sites and result in product selectivity and enhancement in catalytic activity. An ideal catalyst would have a low energy barrier, selectivity towards the desired product, easy synthesis, recoverability and cost-effectiveness.[24] SACs of non-noble metals have all these advantages, which can reduce the process cost while increasing the catalytic performance without compromising selectivity towards desired products.[25,26] Hence, SACs of non-noble metals are the best choice for

CO<sub>2</sub> conversion into value-added products. Carbon dioxide is the major greenhouse gas which leads to climate change and global warming. Thus, the conversion of CO<sub>2</sub> into value-added products can help achieve sustainability and carbon neutrality. Previous efforts to utilize or capture CO<sub>2</sub> have explored the production of value added products like cyclic carbonates, urea, methanol, etc.. However, owing to its high thermodynamic stability, the conversion of CO<sub>2</sub> requires high pressure and temperature. Also, achieving selectivity towards one product is a desirable goal for CO<sub>2</sub> conversion, otherwise in the case of CO<sub>2</sub> hydrogenation we can produce methanol, methane, formate, formic acid, etc.[27,28]

CO<sub>2</sub> fixation and reaction with epoxides to yield cyclic carbonates has potential to produce many commercial products since there are few undesirable side products.[29] The cycloaddition of CO<sub>2</sub> with epoxides is useful for the synthesis of plastics, cosmetics and adhesives.[30,31] These are useful as intermediates for various synthetic processes and also as electrolytes in lithium-ion batteries. Cyclic carbonates have also been utilized to synthesize commercially significant compounds including polycarbonates, polyurethanes, and dialkyl carbonates etc.[32] Traditionally cyclic carbonates were synthesized using highly toxic phosgene, which is banned in many countries. Hence, the synthesis of cyclic carbonates from cycloaddition reaction of epoxides and carbon dioxide is a promising pathway.

Recently, various metal organic frameworks (MOFs) of Cu[33], Pd@Eu[34], Ca based[35], Yttrium[36], thulium[37], Zn[38,39] and Ln based coordinated polymers[40] have been explored for the CO<sub>2</sub> fixation of epoxides with tetrabutylammonium halogen containing reagent (TBAX) at 70-100°C for 4-24 hours and under solvent-free reaction conditions. Furthermore, CuCo<sub>2</sub>O<sub>4</sub> spinel[30], phenolated lignin NPs[41], ligated Ti coated Bi-oxo cores[42], PABA@ $\alpha$ -Fe<sub>2</sub>O<sub>3</sub>[43] and N,S co-doped bifunctional carbon catalyst[44] were also explored using TBAX at room temperature to 105 °C for 3-24 hours. In all cases moderate to good yield was obtained but the reaction time and TBAX amount required was relatively high even at high reaction temperature. However, ionic liquid-based and halide-free reactions were also reported at 60-90 °C and 12-48 hours reaction times with poor substrate scopes.[29,45,46] Several SACs were recently reported for cycloaddition of CO<sub>2</sub> into epoxides;[47–50] however, these all showed narrow substrate scope or required solvents like DCM and DMF.

Herein, we synthesized a Co/ZrO<sub>2</sub> SAC via a facile coprecipitation method and characterized extensively it with EXAFS, STEM, HAADF and XANES techniques to confirm the presence of single atoms and utilized it for catalytic conversion of epoxides into

cyclic carbonates. The single atom catalyst showed superior catalytic activity compared to undoped  $\text{ZrO}_2$  and  $\text{Co}_3\text{O}_4/\text{ZrO}_2$  catalyst. The  $\text{Co}/\text{ZrO}_2$  SAC showed 100% conversion into cyclic carbonate product with minimal amount of TBAB (0.06 mmol) in solvent-free conditions which makes it cost-effective, greener, and environmentally benign[43,51], whereas undoped  $\text{ZrO}_2$  and  $\text{Co}_3\text{O}_4/\text{ZrO}_2$  catalyst showed less than 50% conversion, confirming that the single atom catalyst provides more active sites. The catalyst showed broad substrate scope with excellent yield in all the cases with recyclability of up to six cycles.

## **2. Experimental Section**

### **2.1 Materials**

Cobalt nitrate hexahydrate ( $\text{Co}(\text{NO}_3)_2 \cdot 6\text{H}_2\text{O}$ )  $\geq 99\%$  pure and zirconyl nitrate hydrate ( $\text{ZrO}(\text{NO}_3)_2 \cdot x\text{H}_2\text{O}$ ) anhydrous  $\geq 99.99\%$  pure were purchased from SRL chemicals, India. Ammonia solution was purchased from Merck, India. Reagents and epoxides compounds  $\geq 98\text{-}100\%$  pure were purchased from Sigma-Aldrich and TCI, India. All solvents were used as received.

### **2.2 Catalyst Synthesis**

#### **2.2.1 Synthesis of Co doped $\text{ZrO}_2$**

For synthesizing Co doped  $\text{ZrO}_2$ , firstly Cobalt nitrate hexahydrate and Zirconyl nitrates hydrates (1:9 molar ratio) were taken in round bottom flask in 50 mL water and stirred the mixture for 20 minutes. To maintain the  $\text{pH} \sim 9$ , ammonia solution was added dropwise with continuous stirring. During this addition of ammonia solution colour changes from light pink to bluish pink colour. After stirring the mixture for next 1 hour, the solution was centrifuged and washed several times with water till  $\text{pH} \sim 7$  and then dried overnight at 100 °C. Thereafter, the solid precipitate was calcined at 500 °C for 3 hours with ramping temperature 2 °C/min. The synthesized catalyst is named as  $\text{Co}/\text{ZrO}_2$  single atom catalyst.

#### **2.2.2 Synthesis of undoped $\text{ZrO}_2$**

The undoped  $\text{ZrO}_2$  catalyst was synthesized using zirconyl nitrate with above mentioned method without using cobalt nitrate.

### **2.2.3 Synthesis of $\text{Co}_3\text{O}_4$ supported on $\text{ZrO}_2$**

For synthesizing cobalt impregnated  $\text{ZrO}_2$  catalyst, as synthesized  $\text{ZrO}_2$  was initially taken in round bottom flask and stirred it into water for 20 minutes at room temperature. In another beaker,  $\text{Co}(\text{NO}_3)_2 \cdot 6\text{H}_2\text{O}$  was dissolved in 10 mL water and added dropwise to the above dispersed solution of  $\text{ZrO}_2$  and allowed to stir the mixture for another 1 hour. After 1 hour, the solution was evaporated under reduced pressure and the precipitates were dried overnight at 100 °C and then calcined at 500 °C for 3 hours with ramping temperature 2 °C/min. The synthesized catalyst is named as  $\text{Co}_3\text{O}_4/\text{ZrO}_2$  catalyst.

### **2.3. General catalytic reaction**

In a general  $\text{CO}_2$  fixation reaction, epoxide substrates (10 mmol) were added with catalyst (15 mg), TBAB (0.06 mmol) in stainless steel containing Teflon reaction vessel pressure reactor attached with thermocouple at magnetic stirring bar. After closing the reactor, the reaction vessel was flushed three times with  $\text{CO}_2$  to replace the existing air and then pressurized with 2 bar pressure and keep it for stirring at 80 °C for required reaction time.

After completion of reaction, the reactor was cooled down to room temperature and pressure was released. The reaction mixture was centrifuged for catalyst separation and in the obtained reaction mixture, 0.1 mmol (14  $\mu\text{L}$ ) mesitylene as internal standard was added and diluted with methanol and given for GC-MS analysis to analyze the conversion and selectivity. For NMR analysis, the reaction mixture was diluted with ethyl acetate and dried under rotavapor and then given for analysis to confirm the product formation. Additionally, for recycle study, the centrifuged catalyst was then washed, dried overnight at room temperature, and used for next cycle.

### **2.4. Physicochemical characterization**

Powder x-ray diffraction (PXRD) of the nanoparticle performed using  $\text{Cu K}\alpha$  radiation (1.54 Å) using the Rigaku Smart Lab X-ray diffractometer. Thermogravimetric analysis was performed using METTLER TOLEDO (TGA/DSC 1) to evaluate the thermal stability of SAC. The Brunauer–Emmett–Teller (BET) surface area was determined using  $\text{N}_2$  and  $\text{CO}_2$  adsorption-desorption measurements. The morphology was analysed by using Supra55 Zeiss Field Emission Scanning Electron Microscopy (Supra55 Zeiss FE-SEM) and FEI Tecnai G2 F30 Field Emission Gun-Transmission Electron Microscopy (HR-TEM, operable at 300 kV). The X-ray Photoelectron Spectroscopy (XPS) analysis of fresh catalysts was recorded using Scient Omicron Multiprobe MXPS spectrometer.

Samples were dispersed in ethanol and mounted on holey carbon grids for examination in a JEOL NEOARM 200CF transmission electron microscope equipped with spherical aberration correction to allow atomic resolution imaging, and an Oxford Aztec Energy Dispersive System (EDS) for elemental analysis. The microscope is equipped with two large area JEOL EDS detectors for higher throughput in acquisition of x-ray fluorescence signals. Images were recorded in annular dark field (ADF) mode and in annular bright field (ABF) mode.

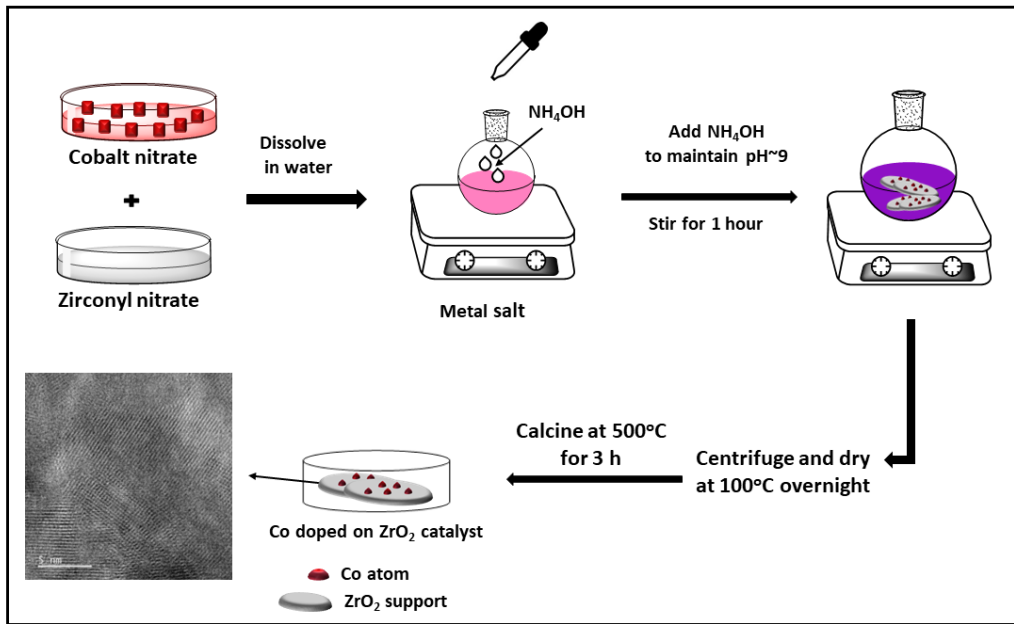
XAS experiments were performed at 5BM-D beamline of DND-CAT at beamline 5 BM-D (DND-CAT) of the Advanced Photon Source (APS) of Argonne National Laboratory, at Co K (7709 eV) edge. Co/ZrO<sub>2</sub> and Co<sub>3</sub>O<sub>4</sub>/ZrO<sub>2</sub> samples were ground to a fine powder by using a pestle and mortar, then evenly spread on long Scotch tape (3M Corp) to form a uniform sample layer. The tape was folded to create a uniform surface to produce adequate absorption. The sample was mounted vertically on a sample holder with its surface normal bisecting the 90° angles between the X-ray incidence and photon detecting directions. A double crystal Si (111) monochromator was used for energy selection. Both Co K-edge XANES and EXAFS were measured under fluorescence mode by a Vortex ME4 detector. Metal Co foil transmission spectrum for energy calibration was collected along with each sample. XAS data were processed using WinXAS software.[52] Simulated phase and amplitude functions for Co-O scattering were extracted using Feff6.[53] The extracted *chi* was *k*<sup>2</sup>-weighted and Fourier transformed over a *k* range of 2.5 to 10 Å<sup>-1</sup> for the samples. The S<sub>0</sub><sup>2</sup> value was determined by fitting the Co foil reference compound. Fitting was performed in *q*-space to determine the Debye-Waller factor, Δσ<sup>2</sup>. The final EXAFS fits were conducted in *R*-space.

The catalyst leaching was performed using ICP-Atomic Emission Spectroscopy (Model: ARCOS, Simultaneous ICP Spectrometer). Identification of the products of catalytic reactions carried out using Shimadzu GC-MS, QP2010 mass spectrometer with a 30 m long Rxi-5Sil MS separation column with a 0.25 mm diameter and 0.25 μM thickness. The formation of substituted products was confirmed by <sup>1</sup>H and <sup>13</sup>C NMR analysis using NMR Spectrometer, Model AVANCE NEO Ascend 500 Bruker BioSpin International AG.

### 3. Results and discussion

#### 3.1 Characterization of catalyst

The single-atom catalyst Co/ZrO<sub>2</sub> was synthesized via coprecipitation method[54] as shown in **Scheme 1**. For comparison, undoped ZrO<sub>2</sub> and Co<sub>3</sub>O<sub>4</sub> impregnated ZrO<sub>2</sub> was synthesized via incipient wetness impregnation.



**Scheme 1.** Schematic representation of the synthesis of Co/ZrO<sub>2</sub> catalyst.

All three catalysts i.e., single atom Co/ZrO<sub>2</sub> catalyst, undoped ZrO<sub>2</sub> and Co<sub>3</sub>O<sub>4</sub>/ZrO<sub>2</sub> catalyst were characterized using powder X-ray diffraction as shown in **Figure 1**. As shown in **Figure 1A**, undoped ZrO<sub>2</sub> catalyst showed peaks at 30.31°, 35.29°, 50.40°, 60.36° and 63.11° corresponding to the (101), (110), (200), (211) and (202) reflections of tetragonal ZrO<sub>2</sub> in agreement with JCPDS# 01-080-0965.[55,56] In contrast, the cobalt doped catalyst was analysed and there was no peak corresponding to any cobalt phase, which confirms that the Co was doped into the ZrO<sub>2</sub> surface. The XRD pattern shows that there is shift in the (101) plane of ZrO<sub>2</sub> to higher 2θ value, further confirming the doping of cobalt as shown in **Figure 1B**. This peak shift is observed due to a decrease in the interplanar spacing in ZrO<sub>2</sub> due to cobalt doping.[57,58] The ionic radii of Co<sup>2+</sup> is 0.74 Å, less than the ionic radius of 0.84 Å for Zr<sup>4+</sup> and which leads to change in lattice constant and results in shift of *t*-ZrO<sub>2</sub> plane to a higher 2θ value.[59] In the cobalt doped catalyst, no peak of Co<sub>3</sub>O<sub>4</sub> was observed.[60] This absence of cobalt and cobalt oxide peaks in the Co/ZrO<sub>2</sub>, supports the inference of doping of cobalt on the zirconia support. For comparison, Co<sub>3</sub>O<sub>4</sub> impregnated ZrO<sub>2</sub> was also

synthesized (See SI) and analysed, showing sharp peaks at  $36.88^\circ$ ,  $44.95^\circ$ ,  $59.51^\circ$  and  $65.11^\circ$  corresponding to the (311), (400), (511) and (440) planes of  $\text{Co}_3\text{O}_4$  in agreement with JCPDS# 043-1003 as shown in **Figure 1A**.<sup>[61,62]</sup> When compared with the  $\text{Co}/\text{ZrO}_2$  catalyst, the powder XRD peak of  $\text{Co}_3\text{O}_4$  for (311) plane was absent in case of  $\text{Co}/\text{ZrO}_2$  suggesting the absence of nanoparticles in  $\text{Co}/\text{ZrO}_2$  catalyst.<sup>[63]</sup> The average crystallite size was calculated using the Scherrer equation<sup>[64]</sup> and it was found to be 17 nm, 20 nm and 12 nm for  $\text{Co}/\text{ZrO}_2$ , undoped  $\text{ZrO}_2$  and  $\text{Co}_3\text{O}_4/\text{ZrO}_2$  respectively.

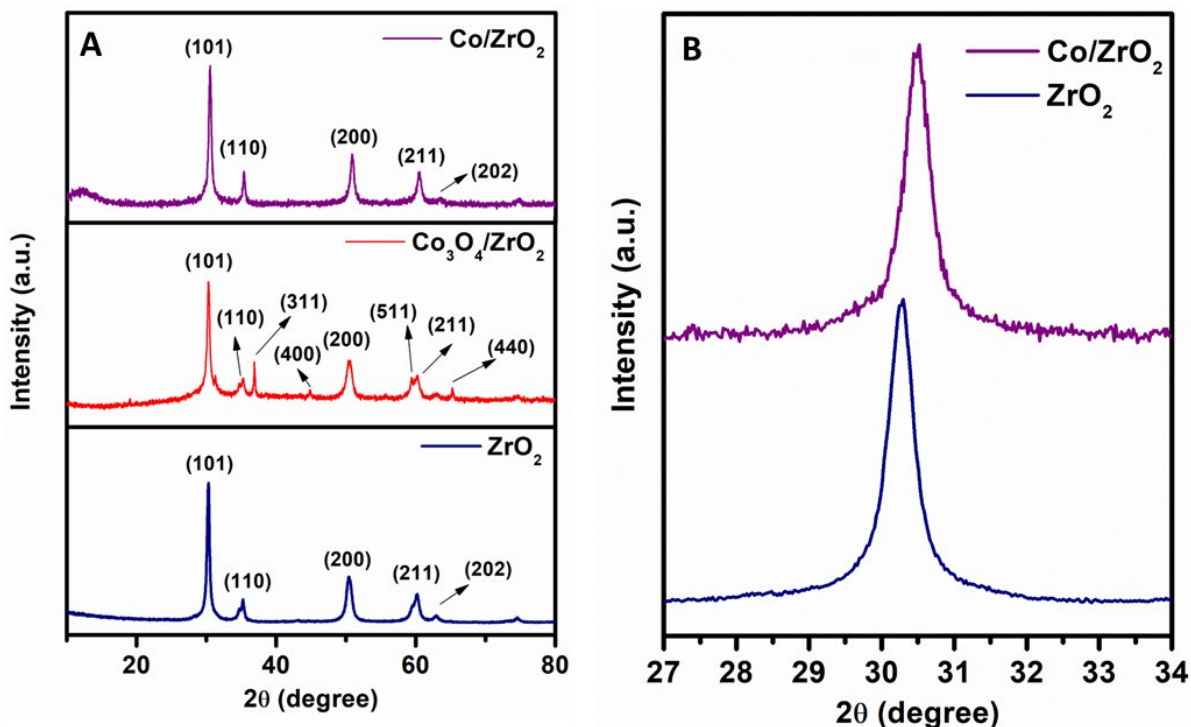


**Figure 1.** (A) PXRD of  $\text{Co}/\text{ZrO}_2$  single atom catalyst,  $\text{Co}_3\text{O}_4$  supported on  $\text{ZrO}_2$  and undoped  $\text{ZrO}_2$  and (B) shifting of (101) plane of  $\text{ZrO}_2$  with doping of cobalt.

The thermal stability of Co doped  $\text{ZrO}_2$  catalyst was analyzed by heating from  $30^\circ\text{C}$  to  $700^\circ\text{C}$  temperature under a nitrogen atmosphere. The thermogravimetric analysis indicates only 4% weight loss, which confirm the high thermal stability of the Co doped  $\text{ZrO}_2$  catalyst as shown in **Figure S1**. There was initial weight loss up to  $200^\circ\text{C}$  due to removal of adsorbed water and further weight loss was observed due to removal of trapped organic species inside the pores of  $\text{ZrO}_2$  support material.<sup>[51]</sup>

$\text{N}_2$  adsorption-desorption was performed at 1 bar pressure at  $77\text{ K}$  temperature after degassing at  $300^\circ\text{C}$  temperature to determine surface area, pore size and pore volume (**Figure S2**). Cobalt doped  $\text{ZrO}_2$  catalyst has a high surface area of  $76\text{ m}^2/\text{g}$  with pore size and pore

volume of 3.4 nm, and 0.061 cc/g respectively. The  $N_2$  adsorption-desorption curve followed a type IV isotherm suggesting the formation of mesopores, which is in good agreement with the Barrett-Joyner-Halenda (BJH) pore size calculated value. Moreover, the undoped  $ZrO_2$  and  $Co_3O_4$  impregnated  $ZrO_2$  was also analyzed, and all three-catalysts showed the same type of isotherm. Moreover, the calculated surface area, pore size and pore volume were found to be  $69\text{ m}^2/\text{g}$ , 3.4 nm and 0.061 cc/g respectively for undoped  $ZrO_2$  (see **Figure S3(A-B)**). Additionally, the specific surface area of  $Co_3O_4/ZrO_2$  catalyst was also calculated using the BET equation and was estimated as  $46\text{ m}^2/\text{g}$  with a pore size and pore volume of 3.4 nm and 0.057 cc/g respectively (see **Figure S3(C-D)**).

To confirm the atomic dispersion of cobalt atom on zirconia, aberration corrected scanning transmission electron microscopy (AC-STEM) was performed. Annular dark field (ADF) and simultaneous annular bright field (ABF) STEM images were recorded as shown in **Figure S4**. In ABF mode, the crystalline morphology of  $ZrO_2$  can be seen clearly as indicated by the lattice fringes (**Figure S4(A-B)**). In ADF mode, there were no identifiable single Co atoms on  $ZrO_2$  as shown in **Figure S4(C-D)** as a result of the lower atomic number of Co relative to Zr.[65,66] It is important to note that no clusters of cobalt oxide were observed anywhere in the Co doped catalyst. Further, to confirm the dispersion of Co, Energy-dispersive X-ray spectroscopy (EDS) was performed in different regions of Co/ $ZrO_2$  at various magnifications, as shown in **Figure S5**. In each elemental map, the cobalt distribution was uniform (i.e.,  $6.6\pm0.4\text{ wt\%}$ ) on  $ZrO_2$  and no detectable Co particles on  $ZrO_2$  were observed in the cobalt map. Similarly, the EDS results of HR-TEM and FE-SEM analysis were consistent for Co distribution on  $ZrO_2$  as shown in **Figure 2** and **Figure S6** respectively, which suggests the atomic dispersion of cobalt on the  $ZrO_2$  support. The lattice fringe of 0.287 nm corresponding to the (101) planes of *t*- $ZrO_2$  are shown in **Figure 2B**, which is in agreement with PXRD spectra of the Co single atom catalyst (**Figure 1**). The colour mapping of Co doped  $ZrO_2$  catalyst showed uniform distribution of Co on  $ZrO_2$  catalyst as shown in **Figure 2C**. The SAED pattern of the Co/ $ZrO_2$  catalyst shows the concentric rings expected from the crystalline zirconia support as shown in **Figure 2D** inset. To confirm the content of Co and Zr metal in Co/ $ZrO_2$  catalyst and  $Co_3O_4/ZrO_2$  catalyst, inductively coupled plasma atomic emission spectroscopy (ICP-AES) was performed which confirmed  $\sim6\text{ wt\%}$  and  $\sim9\text{ wt\%}$  of Co content respectively (**Table S1**).

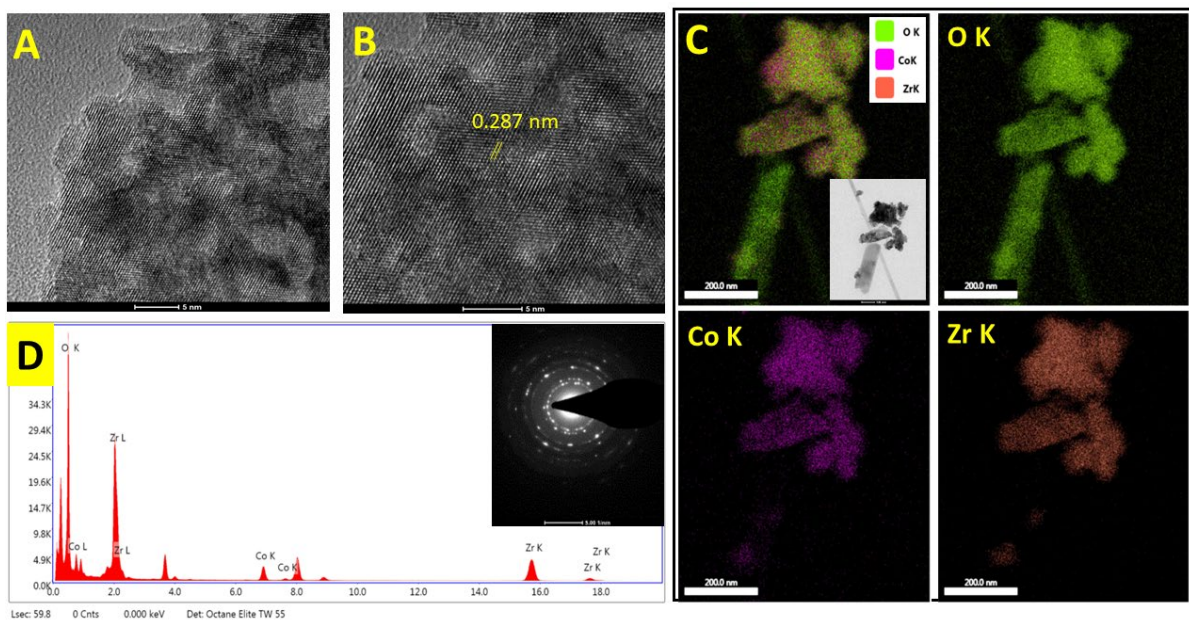


**Figure 2.** HR-TEM images of single atom Co/ZrO<sub>2</sub> catalyst at (A-B) 5 nm, (C) Elemental mapping and (D) EDS spectra (inset selected area electron diffraction (SAED) pattern at 5 1/nm).

For comparison, STEM images of Co<sub>3</sub>O<sub>4</sub> impregnated ZrO<sub>2</sub> were also recorded, which revealed that the catalyst has two types of morphology: one with small pores and the other with more open pore structures as shown in **Figure 3A**. The morphology is quite distinct as seen in this figure and in some cases the two phases are joined to each other, as shown in **Figure 3B**. The EDS analysis shows that the open pore structure comes from the Co<sub>3</sub>O<sub>4</sub> phase since its concentration increases as we zoom into the open pore structure (**Figure 3C and 3D**). The particles of Co<sub>3</sub>O<sub>4</sub> can be as large as the ZrO<sub>2</sub> particles (**Figure S7A**). However, EDS analysis shows that smaller Co<sub>3</sub>O<sub>4</sub> aggregates could be dispersed on the ZrO<sub>2</sub> (**Figure S7C**). Also, in some regions of ZrO<sub>2</sub> there were regions suggestive of atomically dispersed Co (**Figure S7D**). In summary, while the cobalt doped ZrO<sub>2</sub> catalyst contains exclusively atomically dispersed Co, whereas in the impregnated catalyst we see phase separation of Co<sub>3</sub>O<sub>4</sub> and ZrO<sub>2</sub>. Additionally, we also see atomically dispersed Co on the ZrO<sub>2</sub> in the impregnated catalyst. These results are in good agreement with PXRD data where the sharp (311) peak corresponding to large Co<sub>3</sub>O<sub>4</sub> particles in Co<sub>3</sub>O<sub>4</sub>/ZrO<sub>2</sub> is not seen in case of the Co doped on ZrO<sub>2</sub>.

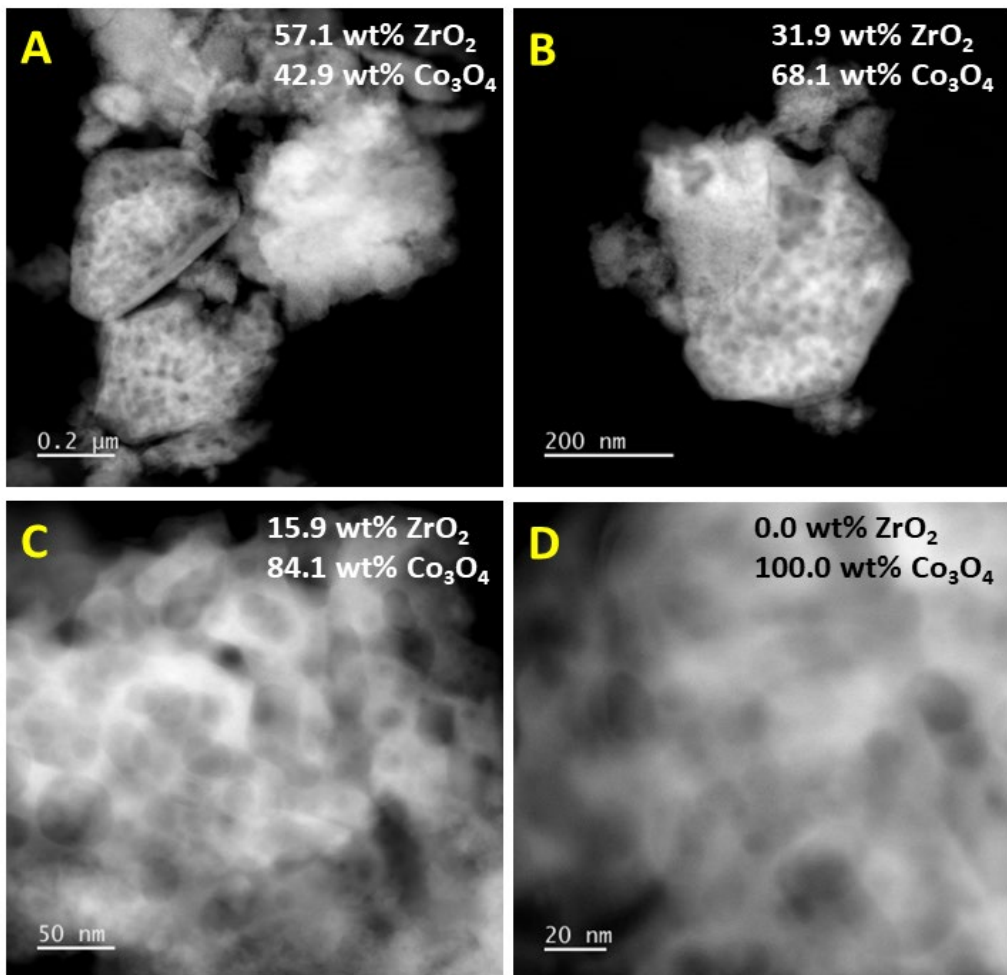


**Figure 3.** (A-B) STEM images of impregnated  $\text{Co}_3\text{O}_4/\text{ZrO}_2$  catalyst at different magnifications as indicated by the scale bars of (A-B) 200 nm, (C) 50 nm, and (D) 20 nm with elemental analysis of each field of view listed on the image.

The local Co coordination and oxidation state were analyzed via Co K-edge X-ray absorption near-edge structure (XANES) and extended X-ray absorption fine structure (EXAFS) spectroscopy, as shown in **Figure 4**. The XANES energy corresponds to the dipole allowed electromagnetic transition for ionization of a 1s electron to the 4p vacant orbitals and is taken as the first inflection point of the leading edge. For 3d compounds, the 1s to 3d dipole forbidden transition gives a pre-edge peak. The energy of the pre-edge peak can be used to determine the oxidation state.[67] The XANES spectra of Co foil (metallic Co) show no obvious pre-edge peak and the leading edge represents the XANES energy at 7709 eV as shown in **Figure 4A**. The  $\text{Co}_3\text{O}_4/\text{ZrO}_2$  reference XANES spectra shows the peak for both  $\text{Co}^{+2}$  and  $\text{Co}^{+3}$  ions.  $\text{Co}^{+2}$  is resolved in the spectrum, while  $\text{Co}^{+3}$  pre-edge peak overlaps with the  $\text{Co}^{+2}$  pre-edge peak and the leading edge of the XANES spectrum as indicated in **Figure 4A**. For  $\text{Co}/\text{ZrO}_2$ , the pre-edge peak has the same energy as  $\text{Co}^{+2}$  with no evidence of a  $\text{Co}^{+3}$

pre-edge peak. Also, the XANES spectrum of Co/ZrO<sub>2</sub> is shifted to lower energy i.e. 7724 eV consistent with Co<sup>+2</sup> ions present on isolated Co<sup>+2</sup> on ZrO<sub>2</sub>.[68,69] Further, Co K-edge EXAFS spectra for Co doped ZrO<sub>2</sub> and Co<sub>3</sub>O<sub>4</sub> impregnated ZrO<sub>2</sub> catalyst were derived as shown in **Figure 4B** and **Figure S8**. The Fourier transform first shell fitting results of Co doped ZrO<sub>2</sub> and Co<sub>3</sub>O<sub>4</sub>/ZrO<sub>2</sub> catalyst along with standard Co<sub>3</sub>O<sub>4</sub> and Co foil are described in **Table 1**.

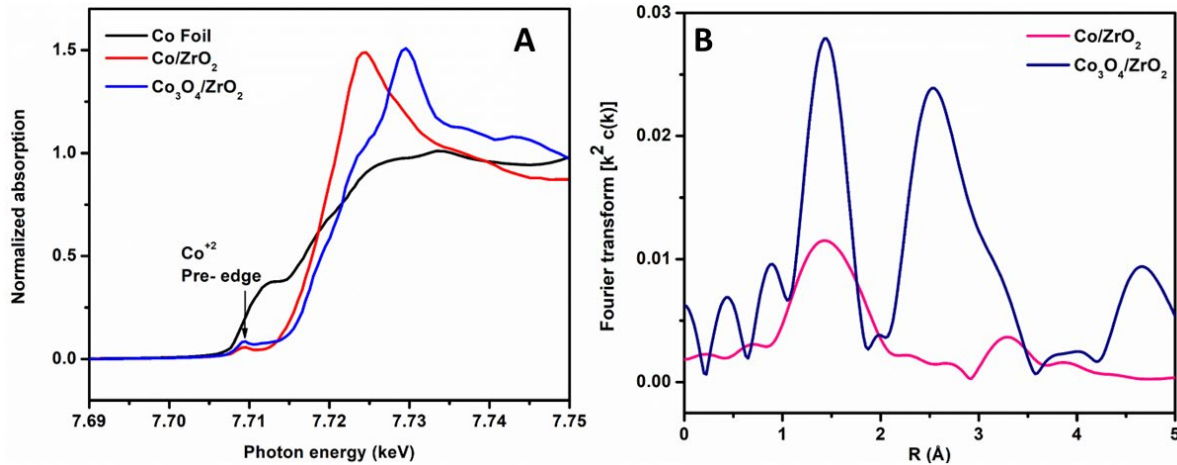


**Figure 4.** (A) Co K-edge XANES spectrum of Co/ZrO<sub>2</sub> single atom catalyst (red), Co<sub>3</sub>O<sub>4</sub>/ZrO<sub>2</sub> impregnated catalyst (blue) along with Co foil (black) as references and (B) Fourier transform of Co K-edge EXAFS spectra of Co/ZrO<sub>2</sub> single atom catalyst where  $k^2: \Delta k = 2.55$  to  $10.0 \text{ \AA}^{-1}$  and Co<sub>3</sub>O<sub>4</sub>/ZrO<sub>2</sub> catalyst where  $k^2: \Delta k = 2.7$  to  $10.2 \text{ \AA}^{-1}$  in R- space.

EXAFS first-shell fitting results indicate 4 Co-O bonds at 2.03 Å of Co/ZrO<sub>2</sub>. For comparison, there are 6 Co-O bonds at 2.13 Å in the CoO reference, while half of the Co in Co<sub>3</sub>O<sub>4</sub> has 4 Co-O at 1.94 Å and 6 Co-O at 1.92 Å with higher shell Co-O-Co peaks at 2.86 and 3.31 Å. Thus, the Co-O bond distance in Co/ZrO<sub>2</sub> is shorter and number of bonds is smaller than those in the CoO reference. In Co/ZrO<sub>2</sub>, there is also a very small second-shell Co-O-Zr peak at 3.42 Å indicating isolated Co<sup>+2</sup> ions. Co<sub>3</sub>O<sub>4</sub>/ZrO<sub>2</sub> has 50% Co with 4 bonds and 50% Co with 6 bonds for an average Co-O coordination of 5 at 1.91 Å. In addition, there are two Co-O-Co higher shell bond distances at 2.87 Å and 3.38 Å consistent with Co<sub>3</sub>O<sub>4</sub> oxide nanoparticles. The EXAFS fits are given in **Table 1**. These results confirmed that Co/ZrO<sub>2</sub> catalysts have no structure reminiscent of CoO and Co<sub>3</sub>O<sub>4</sub> confirming the presence of isolated Co<sup>+2</sup> in the Co doped ZrO<sub>2</sub> single atom catalyst. Furthermore, for comparison Co K-edge EXAFS and XANES spectra of Co<sub>3</sub>O<sub>4</sub>/ZrO<sub>2</sub> with standard Co<sub>3</sub>O<sub>4</sub> was also fitted (Figure S9 and Table 1) where the XANES and EXAFS of Co<sub>3</sub>O<sub>4</sub> and Co<sub>3</sub>O<sub>4</sub>/ZrO<sub>2</sub> have very similar. The small differences are due to the lower Co concentration in the Co<sub>3</sub>O<sub>4</sub>/ZrO<sub>2</sub>

catalyst and the strong absorption of the Co X-rays by  $\text{ZrO}_2$ . All features differ only by the weaker signal of the catalyst as shown in **Table 1**.

**Table 1.** Co K-edge first shell EXAFS fitting results for  $\text{Co/ZrO}_2$ ,  $\text{Co}_3\text{O}_4/\text{ZrO}_2$ ,  $\text{Co}_3\text{O}_4$  and reference Co foil where ( $k^2$ :  $\Delta k = 2.55$  to  $10.0 \text{ \AA}^{-1}$  for  $\text{Co/ZrO}_2$ ,  $k^2$ :  $\Delta k = 2.7 - 12.0 \text{ \AA}^{-1}$  for  $\text{Co}_3\text{O}_4/\text{ZrO}_2$  and  $\Delta R = 1.0 - 3.4 \text{ \AA}$ ) and  ${}^*S_o = 0.80$

Sample	XANES Pre-Edge Energy (eV)	Edge Energy (eV)	Scatter	CN	R ( $\text{\AA}$ )	$\Delta E_o$ (eV)	$\sigma^2$
Co foil*	-	7709.0	Co-Co	12.0	2.49	5.7	0.0065
$\text{Co}_3\text{O}_4$	7709.3	7717.6	Co-O	5.0	1.92	-0.7	0.004
			Co-O-Co	4.4	2.85	-4.8	0.004
			Co-O-Co	5.5	3.35	-6.0	0.004
$\text{Co}_3\text{O}_4/\text{ZrO}_2$	7709.3	7717.6	Co-O	4.8	1.92	0.6	0.005
			Co-O-Co	4.4	2.85	-3.1	0.005
			Co-O-Co	5.0	3.35	-4.4	0.005
$\text{Co/ZrO}_2$	7709.3	7716.4	Co-O	3.9	2.04	-1.3	0.012
			Co-O-Zr	3.7	3.42	1.2	0.016

Confidence Limits for non-overlapping peaks, e.g.,  $\text{Co/ZrO}_2$ : Co-O:  $N = \pm 0.2$ ;  $R = \pm 0.005$ ;  $\sigma^2 = \pm 0.0005$ ; Co-O-Zr:  $N = \pm 0.15$ ,  $R = \pm 0.002$ ;  $\sigma^2 = \pm 0.0006$

Additionally, the X-ray photoelectron spectra (XPS) of the  $\text{Co/ZrO}_2$  catalyst were obtained. The XPS spectra of Co 2p, Zr 3d and O 1s is shown in **Figure 5**. We deconvoluted the XPS spectra (Figure 5), where 284.8 eV was taken as reference energy. The Co 2p spectra display two peaks at 781.4 eV and 796.6 eV for Co 2p<sub>3/2</sub> and Co 2p<sub>1/2</sub> respectively, indicating the presence of  $\text{Co}^{+2}$  shown in **Figure 5A**.<sup>[70–72]</sup> The Zr 3d spectra exhibited two peaks at 182.4 eV and 184.7 eV for Zr 3d<sub>5/2</sub> and Zr 3d<sub>3/2</sub> for tetragonal  $\text{Zr}^{+4}$  as shown in **Figure 5B**.<sup>[25]</sup> As shown in **Figure 5C**, O 1s spectra exhibited two deconvoluted peaks at 530.5 eV and 532.05 eV assigned to lattice oxygen and -OH species on the surface or oxygen vacancies, respectively.<sup>[73–75]</sup>

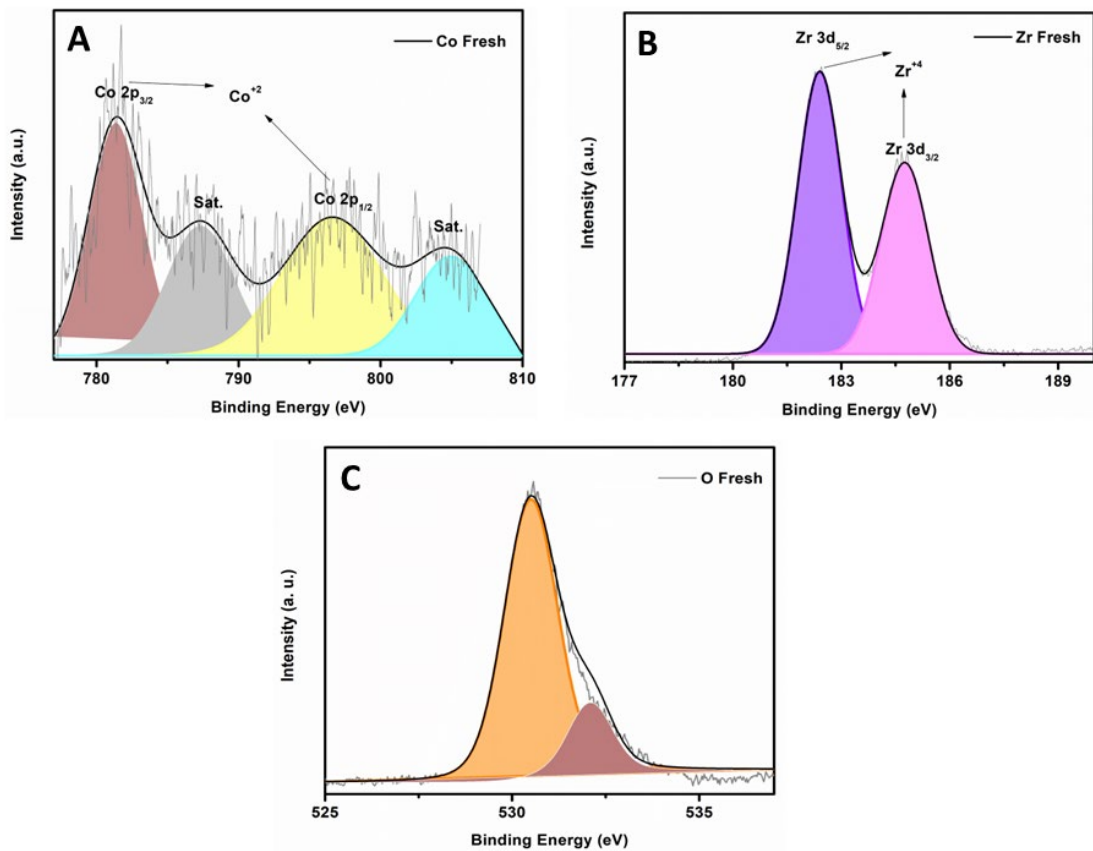
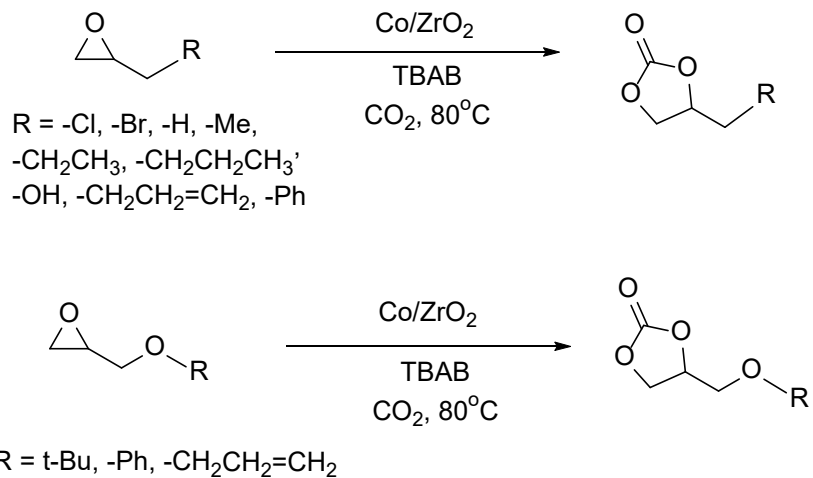


**Figure 5.** XPS analysis of fresh single atom Co/ZrO<sub>2</sub> catalyst **(A)** Co 2p spectrum and **(B)** Zr 2p spectrum and **(C)** O 1s spectrum.

All characterization results are therefore consistent with the Co doped ZrO<sub>2</sub> being a single atom catalyst with uniform isolated Co<sup>+</sup><sup>2</sup> ions with no of Co<sub>3</sub>O<sub>4</sub> or CoO clusters. The impregnated catalyst has a mixed structure with non-uniform dispersion of Co<sub>3</sub>O<sub>4</sub> on ZrO<sub>2</sub>.

### 3.2 Catalytic CO<sub>2</sub> fixation

The undoped ZrO<sub>2</sub> along with Co/ZrO<sub>2</sub> and Co<sub>3</sub>O<sub>4</sub>/ZrO<sub>2</sub> catalysts were tested for catalytic CO<sub>2</sub> fixation of epoxides to yield cyclic carbonates using tetrabutylammonium bromide (TBAB) as a co-catalyst under solvent-free conditions as shown in **Scheme 2**.



**Scheme 2.** General catalytic reaction of cycloaddition of  $\text{CO}_2$  to epoxides.

The reaction conditions were optimized by varying temperature, substrate, and catalyst amounts and various type of tetra butylammonium halide ion. The effect on conversion is shown in **Figure 6**. For the  $\text{CO}_2$  fixation reaction, epichlorohydrin was utilized as model substrate. Initially, the reaction was performed using 10 mmol of epichlorohydrin with 0.25 mmol of TBAB with using 15 mg of  $\text{Co/ZrO}_2$  catalyst at 80 °C temperature for different reaction times from 1-6 hours as shown in **Figure 6A**. With decreasing the reaction time, the conversion decreases from 100 to 55%, respectively. Additional reactions were performed using different reagents i.e., tetrabutylammonium iodide (TBAI), tetrabutylammonium fluoride (TBAF), tetrabutylammonium bromide (TBAB) and 4-Dimethylaminopyridine (DMAP) for 4 hours as shown in **Figure 6B**. In absence of TBAB, there was no conversion observed indicating that TBAB is essential for the reaction and can be considered as co-catalyst for the reaction. In case of TBAB gave the highest epichlorohydrin conversion i.e., 100% into its cyclic carbonate and other reagents showed less conversion of epichlorohydrin. Hence, further optimizations were conducted using TBAB. The amount of TBAB was optimized by varying the concentration from 0.25 mmol to 0.04 mmol. At 0.04 mmol, conversion was 94% while at 0.06 mmol, the conversion was 100%, see **Figure 6C**. Therefore, 0.06 mmol is the optimum amount for the conversion for 10 mmol of epichlorohydrin into its cyclic carbonate. Addition of DMAP gave 65% epichlorohydrin conversion, which may be due to stronger affinity of nitrogen than that of oxygen with epoxide substrate resulting in lower conversion. It appears that DMAP coordinates with catalyst's acidic sites inhibiting the adsorption of epoxide substrate.[44,76] The amount of catalyst and substrate were optimized for different reaction times as shown in **Figure 6(D-F)**. As the catalyst amount decreases from 15 mg to 5 mg, the conversion

decreases from 100% to 89%. While increasing the substrate amount from 10 mmol to 20 mmol, there is also a decrease in conversion. At room temperature, there is only 30% conversion indicating that higher reaction temperatures are required to affect epoxide, ring-opening and  $\text{CO}_2$  fixation. The optimized reaction conditions were 10 mmol of epichlorohydrin, 12 mg of  $\text{Co}/\text{ZrO}_2$  catalyst, 0.06 mmol of TBAB with 2 bar  $\text{CO}_2$  at 80 °C with solvent-free reaction condition wherein 100% conversion was observed.

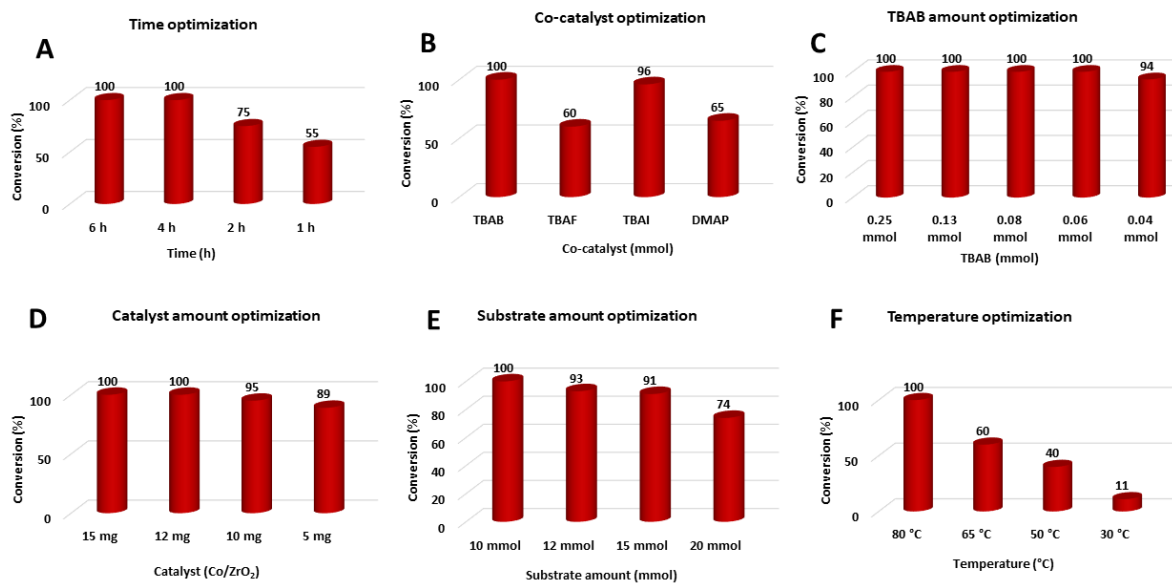


**Figure 6.** Catalytic optimization of  $\text{CO}_2$  fixation reaction at various reaction conditions.

**Reaction conditions:** (A) substrate = 10 mmol, catalyst ( $\text{Co}/\text{ZrO}_2$ ) = 15 mg, TBAB = 0.25 mmol, temperature = 80 °C, time = 1-6 h,  $\text{CO}_2$  = 2 bar. (B) substrate = 10 mmol, catalyst ( $\text{Co}/\text{ZrO}_2$ ) = 15 mg, TBAB = 0.25 mmol, temperature = 80 °C, time = 4 h,  $\text{CO}_2$  = 2 bar. (C) substrate = 10 mmol, catalyst ( $\text{Co}/\text{ZrO}_2$ ) = 15 mg, TBAB = 0.25-0.04 mmol, temperature = 80 °C, time = 4 h,  $\text{CO}_2$  = 2 bar. (D) substrate = 10 mmol, catalyst ( $\text{Co}/\text{ZrO}_2$ ) = 5-15 mg, TBAB = 0.06 mmol, temperature = 80 °C, time = 4 h,  $\text{CO}_2$  = 2 bar. (E) substrate = 10-20 mmol, catalyst ( $\text{Co}/\text{ZrO}_2$ ) = 12 mg, TBAB = 0.06 mmol, temperature = 80 °C, time = 4 h,  $\text{CO}_2$  = 2 bar. (F) substrate = 10 mmol, catalyst ( $\text{Co}/\text{ZrO}_2$ ) = 12 mg, TBAB = 0.06 mmol, temperature = 30-80 °C, time = 4 h,  $\text{CO}_2$  = 2 bar.

The effect of catalyst composition, e.g., undoped  $\text{ZrO}_2$  and  $\text{Co}_3\text{O}_4$  impregnated  $\text{ZrO}_2$ , was also evaluated and is shown in **Figure 7**. For undoped  $\text{ZrO}_2$ , the conversion was 38%; while for  $\text{Co}_3\text{O}_4/\text{ZrO}_2$ , the conversion was 47%. The slightly higher conversion may be due to small fraction of single  $\text{Co}^{+2}$  ions. However, Co doped  $\text{ZrO}_2$  single atom catalyst showed superior catalytic activity over both undoped  $\text{ZrO}_2$  and  $\text{Co}_3\text{O}_4/\text{ZrO}_2$  catalysts. These results revealed that Co doped  $\text{ZrO}_2$  single atom catalyst provides more active sites due to presence

of isolated  $\text{Co}^{+2}$  on  $\text{ZrO}_2$  support is most suitable catalyst for cycloaddition of  $\text{CO}_2$  to cyclic epoxides to yield cyclic carbonate with minimal amount of TBAB under solvent-free conditions.

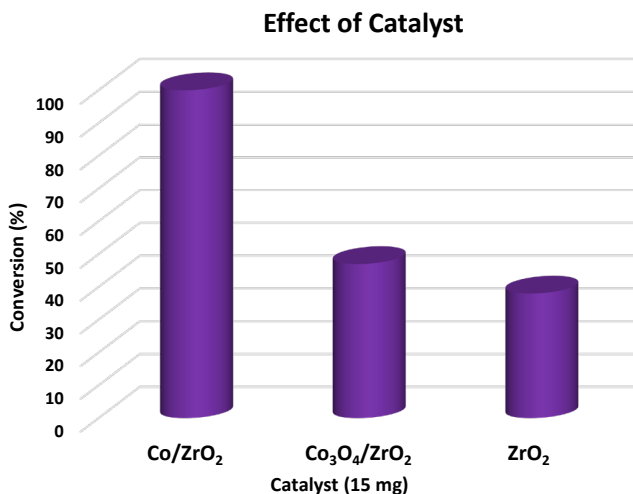


**Figure 7.** Effect of different catalysts on  $\text{CO}_2$  fixation of epichlorohydrin. **Reaction conditions:** Substrate = 10 mmol, catalyst ( $\text{Co/ZrO}_2$ ) = 12 mg,  $\text{CO}_2$  = 2 bar, TBAB = 0.06 mmol (20 mg), temp. = 80 °C, time = 4 h.

To check the scope of the reaction, various substituted epoxides were utilized for the  $\text{CO}_2$  fixation reaction as shown in **Table 2**. All substrates were converted into their corresponding cyclic carbonates at 100% conversion under mild reaction conditions with minimal amount of TBAB. Both -chloro and -bromo substituted epoxides gave 100% conversion into cyclic carbonates in 4-5 hours (**Table 2, Entry 1-2**). Similarly, aliphatic substituted epoxides gave 100% conversion into their corresponding carbonates in 4-7 hours (**Table 2, Entry 3-7**). However, as the aliphatic chain size increases from epoxypropane (propylene oxide) to epoxy hexane, the reaction time increases, perhaps, due to steric hindrance near the epoxide ring.[77] Finally, styrene oxide, allyl glycidyl ether, tert-Butyl glycidyl ether and phenyl glycidyl ether and other aromatic epoxides i.e. 3,6-Dioxabicyclo[3.1.0]hexane were also converted 100% into corresponding carbonates (**Table 2, Entry 8-13**). As the bulky substitute increases, the reaction time increases with decreasing catalytic activity. The effect of the bulky group was observed, in all the substrates, but complete conversions were obtained with 100% selectivity. All the conversion and selectivity were determined using  $^1\text{H}$  and  $^{13}\text{C}$  NMR (**Figure S10**) and the yield was calculated through GC-MS analysis using mesitylene as an internal standard (**Figure S11**).

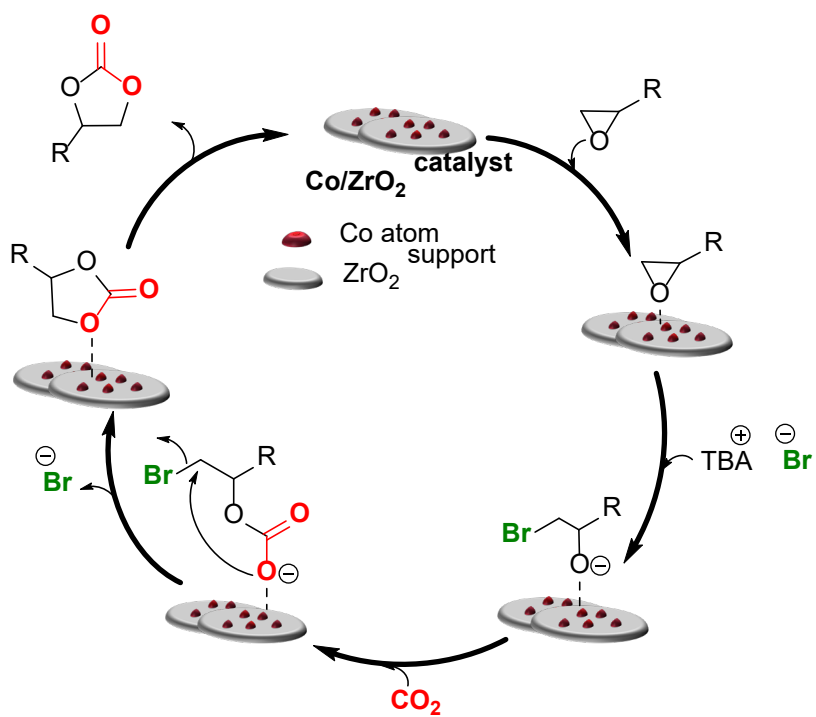
**Table 2.** Substrate scope on CO<sub>2</sub> fixation of epichlorohydrin

Entry	Substrate	Product	Time (h)	Yield <sup>a</sup> (%)	TOF (h <sup>-1</sup> )
1			4	100	37.94
2			5	100	30.35
3			4	100	37.94
4			4	100	37.94
5			6	100	25.29
6			7	100	21.68
7			7	100	21.68
8			8	100	18.97
9			8	100	18.97
10			13	100	11.67
11			12	100	12.65

12			13	100	11.67
13			16	100	9.48

**Reaction conditions:** Substrate = 10 mmol, catalyst ( $\text{Co}/\text{ZrO}_2$ ) = 12 mg, TBAB = 0.06 mmol (20 mg), temperature = 80 °C, time = 4-16 h,  $\text{CO}_2$  = 2 bar. <sup>a</sup>Yield was calculated using GC-MS analysis with mesitylene as an internal standard. All the conversion and selectivity were analysed with  $^1\text{H}$  and  $^{13}\text{C}$  NMR.

Based on previous literature studies, the reaction mechanism of  $\text{CO}_2$  fixation is shown in **Scheme 3**.[30,33,42,46,78–80] Initially, the epoxide substrate interact on the Lewis acidic  $\text{Co}(\text{II})$  of the catalyst with oxygen atom of the epoxide and as a result of this, weakening of C-O bond of epoxide occurs. Here, in  $\text{Co}/\text{ZrO}_2$ , the single  $\text{Co}^{+2}$  ion is the active site. Subsequently, nucleophilic attack of bromide ion of TBAB occurs on the less hindered carbon atom of epoxide, which leads to ring opening of epoxy substrate.[31,45,81] Further, oxygen atom and carbon atom of  $\text{CO}_2$  interact with positively charged cobalt and oxygen atom of epoxide, respectively. Subsequently, with removal of bromide ion cyclic carbonate formed as a product and the catalyst surface is again free for next cycle.



**Scheme 3.** A plausible mechanism of CO<sub>2</sub> fixation of epoxides into cyclic carbonates.

### 3.3. Recycle study and leaching test

To study the recyclability of the catalyst for CO<sub>2</sub> fixation of epichlorohydrin, after completion of reaction, the reactor was cooled to room temperature and reaction mixture was centrifuged and catalyst was settled down and the above solution was filtered. The filtrate was given for GC-MS analysis and the solid residue was washed with water and ethanol several times and dried overnight at room temperature. This solid residue or catalyst was then utilized for the next catalytic cycle. The catalyst was recyclable up to six cycles as shown in **Figure 8**. The decrease in conversion with each regeneration is likely due to small losses in the amount of catalyst during the separation and washing of the catalyst.

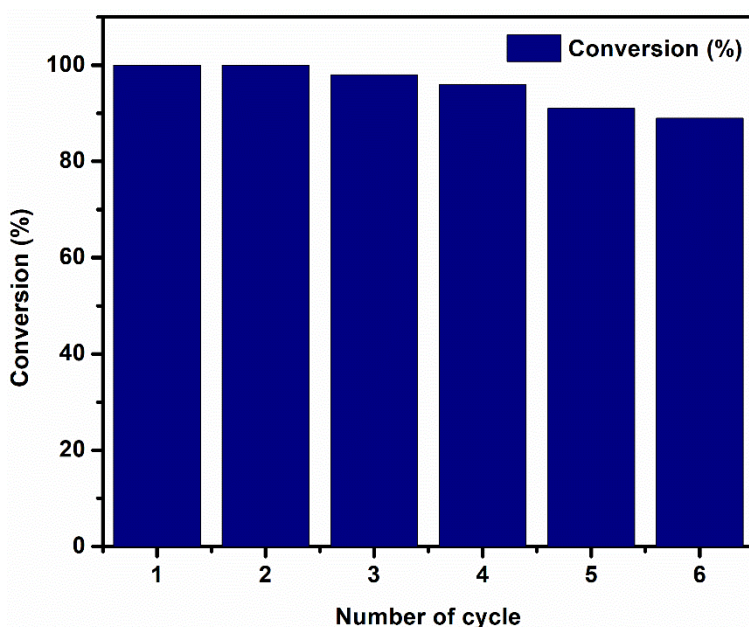


**Figure 8.** Catalyst reusability of the CO<sub>2</sub> fixation in epichlorohydrin for all the cyclic runs.

**Reaction conditions:** Substrate = 10 mmol, catalyst (Co/ZrO<sub>2</sub>) = 12 mg, TBAB = 0.06 mmol (20 mg), temperature = 80 °C, time = 4 h, CO<sub>2</sub> = 2 bar.

Leaching tests of the catalyst were also performed using hot filtration in which the reaction was conducted for 1 hour. After that, reaction mixture was filtered, and the filtrate was allowed to proceed further in presence of CO<sub>2</sub> without catalyst.[51,82] After completion, the conversion and selectivity were determined and confirmed that there was no significant conversion after removal of catalyst. The amount of Co in the filtrate was determined by Inductively Coupled Plasma Atomic Emission Spectroscopy (ICP-AES) and was found less

than 1 ppm, **Table S2**. These studies confirm that the Co doped ZrO<sub>2</sub> single atom catalyst is recyclable for the cycloaddition reaction of CO<sub>2</sub> to epoxides.

In **Table 3**, we compare our results on CO<sub>2</sub> fixation of epoxides with those previously reported in the literature. Cui et al reported zinc single atoms on N-doped carbon via simple pyrolysis of active-carbon-supported phenanthroline-ligated Zn(OAc)<sub>2</sub> complex procedure for cycloaddition of CO<sub>2</sub> and epoxides.[47] The reaction was performed in solvent-free conditions at comparatively high pressure and temperature i.e. 5 bar and 100°C using TBAB as additive. All the substrates (16 substrates) were converted in good to excellent yield, however only 5 mmol of substrate was utilized for the reaction (**Table 3, Entry 1**). Yang et al synthesized a ZIF-8 metal organic framework and derived hollow porous carbon (HPC) with uniform N-doping and loading of Zn SACs via pyrolysis.[48] The reaction was performed with epibromohydrin as substrate under light irradiation at RT, however, reaction was performed in DMF solvent and required 10 hours to achieve 94% conversion (**Table 3, Entry 2**). Li et al synthesized Au<sub>19</sub>Ag<sub>4</sub>(S-Adm)<sub>15</sub> clusters, Au<sub>20</sub>Ag<sub>1</sub>(S-Adm)<sub>15</sub> cluster and Au<sub>21</sub>(S-Adm)<sub>15</sub> with 1-adamantanethiolate (S-Adm).[49] In Au<sub>19</sub>Ag<sub>4</sub>(S-Adm)<sub>15</sub>, all Ag sites are open on surface, in Au<sub>20</sub>Ag<sub>1</sub>(S-Adm)<sub>15</sub> partially open Ag sites and in Au<sub>21</sub>(S-Adm)<sub>15</sub> no Ag sites are present. Based on present Ag sites, their catalytic activity was in order of Au<sub>19</sub>Ag<sub>4</sub>(S-Adm)<sub>15</sub> > Au<sub>20</sub>Ag<sub>1</sub>(S-Adm)<sub>15</sub> > Au<sub>21</sub>(S-Adm)<sub>15</sub>. The reaction was performed with 0.3 mmol of substrates (3 substrates) using DCM/DMF solvent mixture and all three substrates showed ~80% conversion in 24 hours with 10 mol% of TBAB. The reaction involved harmful solvent and involved high reaction time despite the lower amount of substrate (**Table 3, Entry 3-5**). Xu et al explored the strong electronic metal–support interaction in iridium single atom catalyst supported on WO<sub>3</sub> for CO<sub>2</sub> cycloaddition reaction.[50] The reaction was performed in neat condition for 1 mmol of substrate at 40 °C with 10 mg of TBAB. All substrate (6 substrates) were showed moderate to excellent yield (40-100%) in high reaction time i.e., 15 hours (**Table 3, Entry 6**).

Previous literature results utilized either low amounts of substrate with high amount of TBAB and high reaction time or utilized toxic solvents like DCM and DMF. Also, the synthesis process of previous SACs involved multistep procedures whereas our catalyst was synthesized at room temperature with using much simpler methods. Based on this, our results indicate superior catalytic performance with balanced reaction condition for chemical fixation reaction. The Co/ZrO<sub>2</sub> SAC is capable to convert 10 mmol of substrates with trace amount of TBAB (0.06 mmol) with 100% conversion under solvent-free conditions.

**Table 3.** Comparative results of some earlier reported single-atom catalysts

S. No.	Catalyst	Substrate	TBAB	Temp (°C)	Time (h)	Solvent-free	Conv (%)	Ref.
1	Zn-SAC@NC-700	Epichlorohydrin (5 mmol)	2 mol%	100	2	Yes	97	[47]
2	HPC-800 (Zn SACs)	Epibromohydrin (0.15 mmol)	0.1 mmol	300 mW/cm <sup>2</sup>	10	No	94	[48]
3	Au <sub>19</sub> Ag <sub>4</sub> (S-Adm) <sub>15</sub> cluster	Epichlorohydrin (0.3 mmol)	10 mol%	60	24	No	78	[49]
4	Au <sub>20</sub> Ag <sub>1</sub> (S-Adm) <sub>15</sub> cluster	Epichlorohydrin (0.3 mmol)	10 mol%	60	24	No	30	[49]
5	Au <sub>21</sub> (S-Adm) <sub>15</sub> cluster	Epichlorohydrin (0.3 mmol)	10 mol%	60	24	No	50	[49]
6	Ir/WO <sub>3</sub> SAC	Epichlorohydrin (1 mmol)	0.03 mmol	40	15	Yes	100	[50]
7	Co/ZrO <sub>2</sub>	Epichlorohydrin (10 mmol)	0.06 mmol	80	4	Yes	100	This work

#### 4. Conclusions

We have successfully synthesized Co doped  $\text{ZrO}_2$  single atom catalyst via co-precipitation and characterized via STEM, XANES and EXAFS to confirm the Co is present in the form of single atoms. The EXAFS data revealed the presence of isolated  $\text{Co}^{+2}$  ions with 4 Co-O bonds at 2.04 Å. EDS elemental mapping confirmed the uniform dispersion of Co on  $\text{ZrO}_2$  support. The as synthesized single atom catalyst was utilized for  $\text{CO}_2$  fixation into epoxides in solvent-free condition to give high rates and selectivity of cyclic carbonates. For comparison, undoped  $\text{ZrO}_2$  and  $\text{Co}_3\text{O}_4/\text{ZrO}_2$  catalyst were utilized which were much less active for  $\text{CO}_2$  fixation. These results suggest that the single atom  $\text{Co}^{+2}$  catalyst is superior to other reported single atom  $\text{CO}_2$  fixation catalysts.

#### Conflicts of interest

There are no conflicts to declare.

#### Acknowledgements

S.M.M. thanks SERB-DST, New Delhi, India (Project CRG/ 2020/001769), BRNS, Mumbai, India (Project 58/14/17/2020- BRNS/37215), and IIT Indore for financial support. N.C. thanks to UGC, New Delhi for fellowship. We are also thankful to sophisticated instrumentation centre (SIC), IIT-Indore for providing the characterization facilities. We are also thankful to 500 MHz NMR facility at the Department of Chemistry funded by DST-FIST, Government of India. We would also like to acknowledge SAIF, IIT-Bombay for HR-TEM and ICP-AES analysis and MRC at MNIT-Jaipur. Also, we would like to thank MEMS department, IIT-Indore for SEM-EDS analysis. Use of the Advanced Photon Source, an Office of Science user facility, was supported by the U.S. Department of Energy, Office of Science, Office of Basic Energy Sciences under Contract No. DE-AC02-06CH11357. The operation of the 10-BM beamline was supported by the Department of Energy and the MRCAT member institutions. Acquisition of the AC-STEM at UNM was supported by NSF DMR-1828731.

## References:

- [1] H. Zhang, W. Zhou, T. Chen, B.Y. Guan, Z. Li, X.W. (David) Lou, A modular strategy for decorating isolated cobalt atoms into multichannel carbon matrix for electrocatalytic oxygen reduction, *Energy Environ. Sci.* 11 (2018) 1980–1984. <https://doi.org/10.1039/C8EE00901E>.
- [2] Y. Guo, S. Mei, K. Yuan, D.-J. Wang, H.-C. Liu, C.-H. Yan, Y.-W. Zhang, Low-Temperature CO<sub>2</sub> Methanation over CeO<sub>2</sub>-Supported Ru Single Atoms, Nanoclusters, and Nanoparticles Competitively Tuned by Strong Metal–Support Interactions and H-Spillover Effect, *ACS Catal.* 8 (2018) 6203–6215. <https://doi.org/10.1021/acscatal.7b04469>.
- [3] Y. Kwon, T.Y. Kim, G. Kwon, J. Yi, H. Lee, Selective Activation of Methane on Single-Atom Catalyst of Rhodium Dispersed on Zirconia for Direct Conversion, *J. Am. Chem. Soc.* 139 (2017) 17694–17699. <https://doi.org/10.1021/jacs.7b11010>.
- [4] R. Qi, B. Zhu, Z. Han, Y. Gao, High-Throughput Screening of Stable Single-Atom Catalysts in CO<sub>2</sub> Reduction Reactions, *ACS Catal.* 12 (2022) 8269–8278. <https://doi.org/10.1021/acscatal.2c02149>.
- [5] Y. Li, J. Hao, H. Song, F. Zhang, X. Bai, X. Meng, H. Zhang, S. Wang, Y. Hu, J. Ye, Selective light absorber-assisted single nickel atom catalysts for ambient sunlight-driven CO<sub>2</sub> methanation, *Nat Commun.* 10 (2019) 2359. <https://doi.org/10.1038/s41467-019-10304-y>.
- [6] Y. Lu, Z. Zhang, H. Wang, Y. Wang, Toward efficient single-atom catalysts for renewable fuels and chemicals production from biomass and CO<sub>2</sub>, *Applied Catalysis B: Environmental.* 292 (2021) 120162. <https://doi.org/10.1016/j.apcatb.2021.120162>.
- [7] W. Zhang, W. Zheng, Single Atom Excels as the Smallest Functional Material, *Advanced Functional Materials.* 26 (2016) 2988–2993. <https://doi.org/10.1002/adfm.201600240>.
- [8] J. Liu, Catalysis by Supported Single Metal Atoms, *ACS Catal.* 7 (2017) 34–59. <https://doi.org/10.1021/acscatal.6b01534>.
- [9] S. Mitchell, E. Vorobyeva, J. Pérez-Ramírez, The Multifaceted Reactivity of Single-Atom Heterogeneous Catalysts, *Angewandte Chemie International Edition.* 57 (2018) 15316–15329. <https://doi.org/10.1002/anie.201806936>.
- [10] Y. Peng, B. Lu, S. Chen, Carbon-Supported Single Atom Catalysts for Electrochemical Energy Conversion and Storage, *Advanced Materials.* 30 (2018) 1801995. <https://doi.org/10.1002/adma.201801995>.
- [11] S.C. Vasconcelos, L. Marchini, C.G.S. Lima, V.G.C. Madriaga, R.S.A. Ribeiro, V. Rossa, L.E.M. Ferreira, F. de C. da Silva, V.F. Ferreira, F.B. Passos, R.S. Varma, M.W. Paixão, T.M. Lima, Single-atom catalysts for the upgrading of biomass-derived molecules: an overview of their preparation, properties and applications, *Green Chem.* 24 (2022) 2722–2751. <https://doi.org/10.1039/D1GC03809E>.
- [12] A. Wang, J. Li, T. Zhang, Heterogeneous single-atom catalysis, *Nat Rev Chem.* 2 (2018) 65–81. <https://doi.org/10.1038/s41570-018-0010-1>.
- [13] B. Singh, M.B. Gawande, A.D. Kute, R.S. Varma, P. Fornasiero, P. McNeice, R.V. Jagadeesh, M. Beller, R. Zbořil, Single-Atom (Iron-Based) Catalysts: Synthesis and Applications, *Chem. Rev.* 121 (2021) 13620–13697. <https://doi.org/10.1021/acs.chemrev.1c00158>.
- [14] Q. Wu, C. Wu, Mechanism insights on single-atom catalysts for CO<sub>2</sub> conversion, *J. Mater. Chem. A.* 11 (2023) 4876–4906. <https://doi.org/10.1039/D2TA06949K>.
- [15] S. Ji, Y. Chen, X. Wang, Z. Zhang, D. Wang, Y. Li, Chemical Synthesis of Single Atomic Site Catalysts, *Chem. Rev.* 120 (2020) 11900–11955. <https://doi.org/10.1021/acs.chemrev.9b00818>.

[16] Q. Liu, Z. Zhang, Platinum single-atom catalysts: a comparative review towards effective characterization, *Catalysis Science & Technology*. 9 (2019) 4821–4834. <https://doi.org/10.1039/C9CY01028A>.

[17] L. Lin, S. Yao, R. Gao, X. Liang, Q. Yu, Y. Deng, J. Liu, M. Peng, Z. Jiang, S. Li, Y.-W. Li, X.-D. Wen, W. Zhou, D. Ma, A highly CO-tolerant atomically dispersed Pt catalyst for chemoselective hydrogenation, *Nat. Nanotechnol.* 14 (2019) 354–361. <https://doi.org/10.1038/s41565-019-0366-5>.

[18] P. Qi, J. Wang, X. Djitcheu, D. He, H. Liu, Q. Zhang, Techniques for the characterization of single atom catalysts, *RSC Adv.* 12 (2021) 1216–1227. <https://doi.org/10.1039/D1RA07799F>.

[19] L. Gong, D. Zhang, C.-Y. Lin, Y. Zhu, Y. Shen, J. Zhang, X. Han, L. Zhang, Z. Xia, Catalytic Mechanisms and Design Principles for Single-Atom Catalysts in Highly Efficient CO<sub>2</sub> Conversion, *Advanced Energy Materials*. 9 (2019) 1902625. <https://doi.org/10.1002/aenm.201902625>.

[20] M.-M. Millet, G. Algara-Siller, S. Wrabetz, A. Mazheika, F. Girgsdies, D. Teschner, F. Seitz, A. Tarasov, S.V. Levchenko, R. Schlögl, E. Frei, Ni Single Atom Catalysts for CO<sub>2</sub> Activation, *J. Am. Chem. Soc.* 141 (2019) 2451–2461. <https://doi.org/10.1021/jacs.8b11729>.

[21] N. Zhang, X. Zhang, L. Tao, P. Jiang, C. Ye, R. Lin, Z. Huang, A. Li, D. Pang, H. Yan, Y. Wang, P. Xu, S. An, Q. Zhang, L. Liu, S. Du, X. Han, D. Wang, Y. Li, Silver Single-Atom Catalyst for Efficient Electrochemical CO<sub>2</sub> Reduction Synthesized from Thermal Transformation and Surface Reconstruction, *Angewandte Chemie International Edition*. 60 (2021) 6170–6176. <https://doi.org/10.1002/anie.202014718>.

[22] C. Gao, S. Chen, Y. Wang, J. Wang, X. Zheng, J. Zhu, L. Song, W. Zhang, Y. Xiong, Heterogeneous Single-Atom Catalyst for Visible-Light-Driven High-Turnover CO<sub>2</sub> Reduction: The Role of Electron Transfer, *Advanced Materials*. 30 (2018) 1704624. <https://doi.org/10.1002/adma.201704624>.

[23] C. Zhu, S. Fu, Q. Shi, D. Du, Y. Lin, Single-Atom Electrocatalysts, *Angewandte Chemie International Edition*. 56 (2017) 13944–13960. <https://doi.org/10.1002/anie.201703864>.

[24] C. Ling, Q. Li, A. Du, J. Wang, Computation-Aided Design of Single-Atom Catalysts for One-Pot CO<sub>2</sub> Capture, Activation, and Conversion, *ACS Appl. Mater. Interfaces*. 10 (2018) 36866–36872. <https://doi.org/10.1021/acsmami.8b10394>.

[25] X. Xiong, C. Mao, Z. Yang, Q. Zhang, G.I.N. Waterhouse, L. Gu, T. Zhang, Photocatalytic CO<sub>2</sub> Reduction to CO over Ni Single Atoms Supported on Defect-Rich Zirconia, *Advanced Energy Materials*. 10 (2020) 2002928. <https://doi.org/10.1002/aenm.202002928>.

[26] X. Li, A.-E. Surkus, J. Rabeah, M. Anwar, S. Dastigir, H. Junge, A. Brückner, M. Beller, Cobalt Single-Atom Catalysts with High Stability for Selective Dehydrogenation of Formic Acid, *Angewandte Chemie International Edition*. 59 (2020) 15849–15854. <https://doi.org/10.1002/anie.202004125>.

[27] A.M. Abdel-Mageed, S. Wohlrab, Review of CO<sub>2</sub> Reduction on Supported Metals (Alloys) and Single-Atom Catalysts (SACs) for the Use of Green Hydrogen in Power-to-Gas Concepts, *Catalysts*. 12 (2022) 16. <https://doi.org/10.3390/catal12010016>.

[28] K. Rohmann, J. Kothe, M.W. Haenel, U. Englert, M. Hölscher, W. Leitner, Hydrogenation of CO<sub>2</sub> to Formic Acid with a Highly Active Ruthenium Acriphos Complex in DMSO and DMSO/Water, *Angewandte Chemie International Edition*. 55 (2016) 8966–8969. <https://doi.org/10.1002/anie.201603878>.

[29] K. Liu, Z. Xu, H. Huang, Y. Zhang, Y. Liu, Z. Qiu, M. Tong, Z. Long, G. Chen, In situ synthesis of pyridinium-based ionic porous organic polymers with hydroxide anions and

pyridinyl radicals for halogen-free catalytic fixation of atmospheric CO<sub>2</sub>, *Green Chemistry*. 24 (2022) 136–141. <https://doi.org/10.1039/D1GC03465K>.

[30] D. Prasad, K.N. Patil, J.T. Bhanushali, B.M. Nagaraja, A.H. Jadhav, Sustainable fixation of CO<sub>2</sub> into epoxides to form cyclic carbonates using hollow marigold CuCo<sub>2</sub>O<sub>4</sub> spinel microspheres as a robust catalyst, *Catal. Sci. Technol.* 9 (2019) 4393–4412. <https://doi.org/10.1039/C9CY00945K>.

[31] X.-B. Lu, D.J. Dahrensbourg, Cobalt catalysts for the coupling of CO<sub>2</sub> and epoxides to provide polycarbonates and cyclic carbonates, *Chem. Soc. Rev.* 41 (2012) 1462–1484. <https://doi.org/10.1039/C1CS15142H>.

[32] A. Mitra, T. Biswas, S. Ghosh, G. Tudu, K. S. Paliwal, S. Ghosh, V. Mahalingam, Halide-free catalytic carbon dioxide fixation of epoxides to cyclic carbonates under atmospheric pressure, *Sustainable Energy & Fuels.* 6 (2022) 420–429. <https://doi.org/10.1039/D1SE01513C>.

[33] S.N. Ansari, P. Kumar, A.K. Gupta, P. Mathur, S.M. Mobin, Catalytic CO<sub>2</sub> Fixation over a Robust Lactam-Functionalized Cu(II) Metal Organic Framework, *Inorg. Chem.* 58 (2019) 9723–9732. <https://doi.org/10.1021/acs.inorgchem.9b00684>.

[34] L.-X. You, S.-X. Yao, B.-B. Zhao, G. Xiong, I. Dragutan, V. Dragutan, X.-G. Liu, F. Ding, Y.-G. Sun, Striking dual functionality of a novel Pd@Eu-MOF nanocatalyst in C(sp<sup>2</sup>)–C(sp<sup>2</sup>) bond-forming and CO<sub>2</sub> fixation reactions, *Dalton Transactions.* 49 (2020) 6368–6376. <https://doi.org/10.1039/D0DT00770F>.

[35] Y.-X. Wang, H.-M. Wang, P. Meng, D.-X. Song, J.-J. Hou, X.-M. Zhang, An uncoordinated tertiary nitrogen based tricarboxylate calcium network with Lewis acid–base dual catalytic sites for cyanosilylation of aldehydes, *Dalton Trans.* 50 (2021) 1740–1745. <https://doi.org/10.1039/D0DT03747H>.

[36] Y. Ye, B. Ge, X. Meng, Y. Liu, S. Wang, X. Song, Z. Liang, An yttrium-organic framework based on a hexagonal prism second building unit for luminescent sensing of antibiotics and highly effective CO<sub>2</sub> fixation, *Inorg. Chem. Front.* 9 (2022) 391–400. <https://doi.org/10.1039/D1QI01352A>.

[37] H. Chen, Z. Zhang, H. Lv, S. Liu, X. Zhang, Investigation on the catalytic behavior of a novel thulium-organic framework with a planar tetrานuclear {Tm4} cluster as the active center for chemical CO<sub>2</sub> fixation, *Dalton Trans.* 51 (2022) 532–540. <https://doi.org/10.1039/D1DT03646G>.

[38] F.-X. Ma, F.-Q. Mi, M.-J. Sun, T. Huang, Z.-A. Wang, T. Zhang, R. Cao, A highly stable Zn<sub>9</sub>-pyrazolate metal–organic framework with metallosalen ligands as a carbon dioxide cycloaddition catalyst, *Inorg. Chem. Front.* 9 (2022) 1812–1818. <https://doi.org/10.1039/D1QI01555A>.

[39] L. Kong, Z. Li, H. Hu, J. Zhu, Z. Chen, M. Deng, Y. Ling, P. Li, Y. Jia, Y. Zhou, Reticular chemistry approach to explore the catalytic CO<sub>2</sub>-epoxide cycloaddition reaction over tetrahedral coordination Lewis acidic sites in a Rutile-type Zinc-phosphonocarboxylate framework, *Chemical Engineering Journal.* 427 (2022) 131759. <https://doi.org/10.1016/j.cej.2021.131759>.

[40] M. Sinchow, N. Semakul, T. Konno, A. Rujiwattra, Lanthanide Coordination Polymers through Design for Exceptional Catalytic Performances in CO<sub>2</sub> Cycloaddition Reactions, *ACS Sustainable Chem. Eng.* 9 (2021) 8581–8591. <https://doi.org/10.1021/acssuschemeng.1c01955>.

[41] W. Jaroonwatana, T. Theerathanagorn, M. Theerasilp, S.D. Gobbo, D. Yiamsawas, V. D'Elia, D. Crespy, Nanoparticles of aromatic biopolymers catalyze CO<sub>2</sub> cycloaddition to epoxides under atmospheric conditions, *Sustainable Energy & Fuels.* 5 (2021) 5431–5444. <https://doi.org/10.1039/D1SE01305J>.

[42] Q.-R. Ding, Y. Yu, C. Cao, J. Zhang, L. Zhang, Stepwise assembly and reversible structural transformation of ligated titanium coated bismuth-oxo cores: shell

morphology engineering for enhanced chemical fixation of CO<sub>2</sub>, *Chem. Sci.* 13 (2022) 3395–3401. <https://doi.org/10.1039/D1SC06847D>.

[43] G. Tudu, K.S. Paliwal, S. Ghosh, T. Biswas, H.V.S.R.M. Koppisetti, A. Mitra, V. Mahalingam, para-Aminobenzoic acid-capped hematite as an efficient nanocatalyst for solvent-free CO<sub>2</sub> fixation under atmospheric pressure, *Dalton Trans.* 51 (2022) 1918–1926. <https://doi.org/10.1039/D1DT03821D>.

[44] A. Ghosh, G.N. Reddy, M.S.P. K, S. Chatterjee, S. Bhattacharjee, R. Maitra, S.E. Lyubimov, A.V. Arzumanyan, A. Naumkin, A. Bhaumik, B. Chowdhury, Fabrication of a hollow sphere N,S co-doped bifunctional carbon catalyst for sustainable fixation of CO<sub>2</sub> to cyclic carbonates, *Green Chem.* 24 (2022) 1673–1692. <https://doi.org/10.1039/D1GC04153C>.

[45] Y. Sun, H. Huang, H. Vardhan, B. Aguilera, C. Zhong, J.A. Perman, A.M. Al-Enizi, A. Nafady, S. Ma, Facile Approach to Graft Ionic Liquid into MOF for Improving the Efficiency of CO<sub>2</sub> Chemical Fixation, *ACS Appl. Mater. Interfaces.* 10 (2018) 27124–27130. <https://doi.org/10.1021/acsami.8b08914>.

[46] J. Liang, Y.-Q. Xie, X.-S. Wang, Q. Wang, T.-T. Liu, Y.-B. Huang, R. Cao, An imidazolium-functionalized mesoporous cationic metal-organic framework for cooperative CO<sub>2</sub> fixation into cyclic carbonate, *Chem. Commun.* 54 (2018) 342–345. <https://doi.org/10.1039/C7CC08630J>.

[47] X. Cui, X. Dai, A.-E. Surkus, K. Junge, C. Kreyenschulte, G. Agostini, N. Rockstroh, M. Beller, Zinc single atoms on N-doped carbon: An efficient and stable catalyst for CO<sub>2</sub> fixation and conversion, *Chinese Journal of Catalysis.* 40 (2019) 1679–1685. [https://doi.org/10.1016/S1872-2067\(19\)63316-4](https://doi.org/10.1016/S1872-2067(19)63316-4).

[48] Q. Yang, C.-C. Yang, C.-H. Lin, H.-L. Jiang, Metal–Organic-Framework-Derived Hollow N-Doped Porous Carbon with Ultrahigh Concentrations of Single Zn Atoms for Efficient Carbon Dioxide Conversion, *Angewandte Chemie International Edition.* 58 (2019) 3511–3515. <https://doi.org/10.1002/anie.201813494>.

[49] G. Li, X. Sui, X. Cai, W. Hu, X. Liu, M. Chen, Y. Zhu, Precisely Constructed Silver Active Sites in Gold Nanoclusters for Chemical Fixation of CO<sub>2</sub>, *Angewandte Chemie.* 133 (2021) 10667–10670. <https://doi.org/10.1002/ange.202100071>.

[50] Xu et al, Strong Electronic Metal–Support Interaction between Iridium Single Atoms and a WO<sub>3</sub> Support Promotes Highly Efficient and Robust CO<sub>2</sub> Cycloaddition, *Advanced Materials.* 34 (2022) 2206991. <https://doi.org/10.1002/adma.202206991>.

[51] N. Choudhary, M. Abdelgaid, G. Mpourmpakis, S.M. Mobin, CuNi bimetallic nanocatalyst enables sustainable direct carboxylation reactions, *Molecular Catalysis.* 530 (2022) 112620. <https://doi.org/10.1016/j.mcat.2022.112620>.

[52] T. Ressler, WinXAS: a Program for X-ray Absorption Spectroscopy Data Analysis under MS-Windows, *J. Synchrotron Rad.* 5 (1998) 118–122. <https://doi.org/10.1107/S0909049597019298>.

[53] J.J. Rehr, C.H. Booth, F. Bridges, S.I. Zabinsky, X-ray-absorption fine structure in embedded atoms, *Phys. Rev. B.* 49 (1994) 12347–12350. <https://doi.org/10.1103/PhysRevB.49.12347>.

[54] N.H.M. Dostagir, R. Rattanawan, M. Gao, J. Ota, J. Hasegawa, K. Asakura, A. Fukouka, A. Shrotri, Co Single Atoms in ZrO<sub>2</sub> with Inherent Oxygen Vacancies for Selective Hydrogenation of CO<sub>2</sub> to CO, *ACS Catal.* 11 (2021) 9450–9461. <https://doi.org/10.1021/acscatal.1c02041>.

[55] W.L. Vrijburg, J.W.A. van Helden, A. Parastaei, E. Groeneveld, E.A. Pidko, E.J.M. Hensen, Ceria–zirconia encapsulated Ni nanoparticles for CO<sub>2</sub> methanation, *Catal. Sci. Technol.* 9 (2019) 5001–5010. <https://doi.org/10.1039/C9CY01428D>.

[56] G. Ramírez-García, E.D. la Rosa, T. López-Luke, S. S. Panikar, P. Salas, Controlling trapping states on selective theranostic core@shell (NaYF<sub>4</sub>:Yb,Tm@TiO<sub>2</sub>-ZrO<sub>2</sub>)

nanocomplexes for enhanced NIR-activated photodynamic therapy against breast cancer cells, *Dalton Transactions*. 48 (2019) 9962–9973. <https://doi.org/10.1039/C9DT00482C>.

[57] S. Yu, H. Jin Yun, D. Minzae Lee, J. Yi, Preparation and characterization of Fe-doped  $\text{TiO}_2$  nanoparticles as a support for a high performance CO oxidation catalyst, *Journal of Materials Chemistry*. 22 (2012) 12629–12635. <https://doi.org/10.1039/C2JM30360D>.

[58] J. Li, B. Shen, Z. Hong, B. Lin, B. Gao, Y. Chen, A facile approach to synthesize novel oxygen-doped  $\text{g-C}_3\text{N}_4$  with superior visible-light photoreactivity, *Chemical Communications*. 48 (2012) 12017–12019. <https://doi.org/10.1039/C2CC35862J>.

[59] P.V. Radovanovic, D.R. Gamelin, Electronic Absorption Spectroscopy of Cobalt Ions in Diluted Magnetic Semiconductor Quantum Dots: Demonstration of an Isocrystalline Core/Shell Synthetic Method, *J. Am. Chem. Soc.* 123 (2001) 12207–12214. <https://doi.org/10.1021/ja0115215>.

[60] C. Sheng Chua, D. Ansovini, C.J. Jun Lee, Y. Ting Teng, L. Ting Ong, D. Chi, T.S. Andy Hor, R. Raja, Y.-F. Lim, The effect of crystallinity on photocatalytic performance of  $\text{Co}_3\text{O}_4$  water-splitting cocatalysts, *Physical Chemistry Chemical Physics*. 18 (2016) 5172–5178. <https://doi.org/10.1039/C5CP07589K>.

[61] X. Yan, L. Tian, M. He, X. Chen, Three-Dimensional Crystalline/Amorphous  $\text{Co}/\text{Co}_3\text{O}_4$  Core/Shell Nanosheets as Efficient Electrocatalysts for the Hydrogen Evolution Reaction, *Nano Lett.* 15 (2015) 6015–6021. <https://doi.org/10.1021/acs.nanolett.5b02205>.

[62] Y.-X. Zhou, Y.-Z. Chen, L. Cao, J. Lu, H.-L. Jiang, Conversion of a metal–organic framework to N-doped porous carbon incorporating Co and  $\text{CoO}$  nanoparticles: direct oxidation of alcohols to esters, *Chem. Commun.* 51 (2015) 8292–8295. <https://doi.org/10.1039/C5CC01588J>.

[63] Y. Cao, J. Ge, M. Jiang, F. Zhang, X. Lei, Acid-Etched  $\text{Co}_3\text{O}_4$  Nanoparticles on Nickel Foam: The Highly Reactive (311) Facet and Enriched Defects for Boosting Methanol Oxidation Electrocatalysis, *ACS Appl. Mater. Interfaces*. 13 (2021) 29491–29499. <https://doi.org/10.1021/acsami.1c04045>.

[64] N. Choudhary, T. Ghosh, S.M. Mobin, Ketone Hydrogenation by Using  $\text{ZnO}-\text{Cu}(\text{OH})\text{Cl}/\text{MCM}-41$  with a Splash of Water: An Environmentally Benign Approach, *Chemistry – An Asian Journal*. 15 (2020) 1339–1348. <https://doi.org/10.1002/asia.201901610>.

[65] J. Xing, K. Takeuchi, K. Kamei, T. Nakamuro, K. Harano, E. Nakamura, Atomic-number (Z)-correlated atomic sizes for deciphering electron microscopic molecular images, *Proceedings of the National Academy of Sciences*. 119 (2022) e2114432119. <https://doi.org/10.1073/pnas.2114432119>.

[66] S. Yamashita, J. Kikkawa, K. Yanagisawa, T. Nagai, K. Ishizuka, K. Kimoto, Atomic number dependence of Z contrast in scanning transmission electron microscopy, *Sci Rep.* 8 (2018) 12325. <https://doi.org/10.1038/s41598-018-30941-5>.

[67] J.P. Krogman, J.R. Gallagher, G. Zhang, A.S. Hock, J.T. Miller, C.M. Thomas, Assignment of the oxidation states of Zr and Co in a highly reactive heterobimetallic Zr/Co complex using X-ray absorption spectroscopy (XANES), *Dalton Trans.* 43 (2014) 13852–13857. <https://doi.org/10.1039/C4DT01534G>.

[68] Z. Liu, Z. Xiao, G. Luo, R. Chen, C.-L. Dong, X. Chen, J. Cen, H. Yang, Y. Wang, D. Su, Y. Li, S. Wang, Defects-Induced In-Plane Heterophase in Cobalt Oxide Nanosheets for Oxygen Evolution Reaction, *Small*. 15 (2019) 1904903. <https://doi.org/10.1002/smll.201904903>.

[69] L. Reith, C.A. Triana, F. Pazoki, M. Amiri, M. Nyman, G.R. Patzke, Unraveling Nanoscale Cobalt Oxide Catalysts for the Oxygen Evolution Reaction: Maximum Performance, Minimum Effort, *J. Am. Chem. Soc.* 143 (2021) 15022–15038. <https://doi.org/10.1021/jacs.1c03375>.

[70] P. Zhou, S. Zhang, Z. Ren, X. Tang, K. Zhang, R. Zhou, D. Wu, J. Liao, Y. Zhang, C. Huang, In Situ Cutting of Ammonium Perchlorate Particles by Co-Bipy “scalpel” for High Efficiency Thermal Decomposition, *Advanced Science.* 9 (2022) 2204109. <https://doi.org/10.1002/advs.202204109>.

[71] S. Mia, S.J. P. Varapragasam, A. Baride, C. Balasanthiran, B. Balasubramanian, R. M. Rioux, J. D. Hoefelmeyer, Diffusion doping of cobalt in rod-shape anatase  $TiO_2$  nanocrystals leads to antiferromagnetism, *Nanoscale Advances.* 2 (2020) 4853–4862. <https://doi.org/10.1039/D0NA00640H>.

[72] M.S. Ahmed, B. Choi, Y.-B. Kim, Development of Highly Active Bifunctional Electrocatalyst Using  $Co_3O_4$  on Carbon Nanotubes for Oxygen Reduction and Oxygen Evolution, *Sci Rep.* 8 (2018) 2543. <https://doi.org/10.1038/s41598-018-20974-1>.

[73] A. Sinhamahapatra, J.-P. Jeon, J. Kang, B. Han, J.-S. Yu, Oxygen-Deficient Zirconia ( $ZrO_2-x$ ): A New Material for Solar Light Absorption, *Sci Rep.* 6 (2016) 27218. <https://doi.org/10.1038/srep27218>.

[74] P. Lackner, Z. Zou, S. Mayr, U. Diebold, M. Schmid, Using photoelectron spectroscopy to observe oxygen spillover to zirconia, *Physical Chemistry Chemical Physics.* 21 (2019) 17613–17620. <https://doi.org/10.1039/C9CP03322J>.

[75] P. Lackner, J. Hulva, E.-M. Köck, W. Mayr-Schmöller, J.I. J. Choi, S. Penner, U. Diebold, F. Mittendorfer, J. Redinger, B. Klötzer, G. S. Parkinson, M. Schmid, Water adsorption at zirconia: from the  $ZrO_2$  (111)/ $Pt$  3  $Zr(0001)$  model system to powder samples, *Journal of Materials Chemistry A.* 6 (2018) 17587–17601. <https://doi.org/10.1039/C8TA04137G>.

[76] O.P. Klenov, N.A. Chumakova, S.A. Pokrovskaya, A.S. Noskov, Modeling of Heat Transfer in a Porous Monolith Catalyst with Square Channels, *Ind. Eng. Chem. Res.* 55 (2016) 3879–3889. <https://doi.org/10.1021/acs.iecr.5b04804>.

[77] X. Chen, M. Wei, A. Yang, F. Jiang, B. Li, O.A. Kholdeeva, L. Wu, Near-Infrared Photothermal Catalysis for Enhanced Conversion of Carbon Dioxide under Mild Conditions, *ACS Appl. Mater. Interfaces.* 14 (2022) 5194–5202. <https://doi.org/10.1021/acsami.1c18889>.

[78] L.-H. Liu, L. Liu, H.-R. Chi, C.-N. Li, Z.-B. Han, A  $[(M_2)_6L_8]$  metal–organic polyhedron with high  $CO_2$  uptake and efficient chemical conversion of  $CO_2$  under ambient conditions, *Chemical Communications.* 58 (2022) 6417–6420. <https://doi.org/10.1039/D2CC01734B>.

[79] G. Zhai, Y. Liu, L. Lei, J. Wang, Z. Wang, Z. Zheng, P. Wang, H. Cheng, Y. Dai, B. Huang, Light-Promoted  $CO_2$  Conversion from Epoxides to Cyclic Carbonates at Ambient Conditions over a Bi-Based Metal–Organic Framework, *ACS Catal.* 11 (2021) 1988–1994. <https://doi.org/10.1021/acscatal.0c05145>.

[80] S.-C. Ke, T.-T. Luo, G.-G. Chang, K.-X. Huang, J.-X. Li, X.-C. Ma, J. Wu, J. Chen, X.-Y. Yang, Spatially Ordered Arrangement of Multifunctional Sites at Molecule Level in a Single Catalyst for Tandem Synthesis of Cyclic Carbonates, *Inorg. Chem.* 59 (2020) 1736–1745. <https://doi.org/10.1021/acs.inorgchem.9b02952>.

[81] Y. Jung, T. Shin, K. Kim, H. Byun, S.J. Cho, H. Kim, H. Song,  $Rh(0)/Rh(III)$  core–shell nanoparticles as heterogeneous catalysts for cyclic carbonate synthesis, *Chem. Commun.* 53 (2016) 384–387. <https://doi.org/10.1039/C6CC08318H>.

[82] T. Ghosh, P. Chandra, A. Mohammad, S.M. Mobin, Benign approach for methyl-esterification of oxygenated organic compounds using TBHP as methylating and oxidizing agent, *Applied Catalysis B: Environmental.* 226 (2018) 278–288. <https://doi.org/10.1016/j.apcatb.2017.12.056>.